1997; Stewart et al. 2004) was limited to the boundary of proliferative and hypertrophic zones in the wild-type growth plate (Fig. 3A, α-$p57^{Kip2}$), whereas in KMI the $p57^{Kip2}$-expressing cells were broadly and sporadically scattered in the intermediate layer, suggesting a loss of synchronized withdrawal from the cell cycle of the chondrocytes. Hence, the intermediate layer chondrocytes were abnormal cells that had ceased proliferation but had not started hypertrophic differentiation.

To examine whether cGKII has an important role generally for endochondral ossification, we compared the healing process of bone fracture produced by a transverse osteotomy and stabilized with an intramedullary nail at the midshaft of tibiae of wild type and KMI (Shimoaka et al. 2004). X-ray analysis 2 wk after the fracture showed substantial calcified callus formation in wild type, which was rarely seen in KMI (Fig. 3B, X-ray). Time course analyses of the calcified area and the bone mineral content (BMC) of the callus measured by a bone densitometer revealed the impairment of endochondral ossification in KMI at 2 wk and thereafter (Fig. 3C). Histological analysis at 2 wk confirmed that endochondral ossification was present in the wild-type fracture callus; in KMI, however, massive uncalcified cartilagenous callus remained, although intramembranous ossification from the periosteum was normally seen (Fig. 3B, HE). When distributions of hypertrophic and proliferating chondrocytes were examined by the COL10 immunostaining and the BrdU uptake, respectively, the two kinds of cells were located adjacent to each other in the wild-type callus, indicating the tight coupling between proliferation and hypertrophic differentiation in this model as well (Fig. 3B, α-COL10 and BrdU). In the KMI callus, there was an intermediate layer with an accumulation of abnormal cells that were stained by neither marker (Fig. 3B, black bars), as observed in the growth plate.

Taking these histological findings together, the cessation of proliferation and the start of hypertrophic differentiation, which were tightly coupled under normal conditions, were dissociated in both the growth plate and the fracture callus of KMI. The cGKII dysfunction was therefore shown to impair the synchronized switching from proliferation to hypertrophic differentiation of chondrocytes in the endochondral ossification.

Functions of cultured chondrocytes from KMI growth plate

To investigate the mechanism underlying the abnormality of chondrocytes due to the cGKII deficiency, ex vivo cultures of primary chondrocytes isolated from the proximal growth plates of the wild-type and KMI tibiae were performed. We first compared the time course of cell proliferation determined by the growth curve for 8 d, and found no significant difference between wild-type and KMI chondrocytes (Fig. 4A). However, after 5 d of culture when the chondrocytes became confluent, the cell shape by the phase contrast image was different between wild type and KMI: The former was hexagonal whereas the latter showed a spindle-shape appearance (Fig. 4B). ALP staining revealed that the KMI chondrocytes were less differentiated than wild type. In addition, a real-time RT–PCR analysis revealed that the expression of COL10, a marker for hypertrophic differentiation, was down-regulated in cultured KMI chondrocytes compared to wild-type chondrocytes. To confirm the contribution of cGKII to these abnormalities, cGKII was introduced into cultured KMI chondrocytes using an adenovirus vector carrying the *cGKII* gene (Ax-*cGKII*). As a result, the suppression of all of these differentiation markers in the KMI culture was restored to those similar to the wild-type culture, although introduction of the same adenovirus vector without the *cGKII* gene (Ax-vector) did not affect them (Fig. 4B).

We next examined the involvement of cGKII in the putative signalings which regulate hypertrophic differentiation of chondrocytes (Fig. 4C,D). PTH/PTHrP via the cAMP-dependent protein kinase (PKA) is known to be a major signal in the inhibition of chondrocyte hypertrophy (Chung and Kronenberg 2000). PTHrP and PTH/PTHrP receptor levels were similar between the wild-type and KMI cultures, and PTH/PTHrP signaling determined by the dose-response effect of PTH on cAMP accumulation was not enhanced in the KMI chondrocyte culture compared to the wild-type culture, indicating that the impaired differentiation of the KMI chondrocytes is not due to a defect of the inhibition by cGKII on the PTH/PTHrP signaling (Fig. 4C). C-type natriuretic peptide (CNP) is also known to be a positive regulator of endochondral ossification and a putative ligand for cGKII (Chusho et al. 2001; Miyazawa et al. 2002). Addition of CNP failed to rescue either the impaired ALP activity or the COL10 expression in the KMI chondrocyte culture (Fig. 4D), indicating that cGKII plays a role in CNP-mediated chondrocyte differentiation. On the other hand, BMP-2 potently increased these differentiation markers, suggesting that the BMP signaling molecules Smads and Runx2 may be independent of the cGKII signaling (Fig. 4D). These results demonstrate that cGKII is not involved in the two major signalings of chondrocyte hypertrophy: PTH/PTHrP and BMP.

cGKII as an attenuator of Sox9 function

We further examined the involvement of cGKII in the function of Sox9, a transcription factor that is known to be essential for chondrogenic differentiation of mesenchymal cells (de Crombrugghe et al. 2001). Sox9 also functions as a potent inhibitor of the hypertrophic differentiation of chondrocytes (Akiyama et al. 2002), and the expression disappears at the hypertrophic zone in the growth plate (Huang et al. 2000). In line with previous studies, our immunohistochemical study confirmed the lack of Sox9 localization in the hypertrophic zone of the wild-type growth plate; however, nuclear localization of Sox9 was clearly visible in the abnormal intermediate layer of the KMI growth plate (Fig. 5A).

To assess the possible interaction between cGKII and Sox9, we performed transfection experiments with plasmids encoding cGKII and/or Sox9 in cell culture sys-

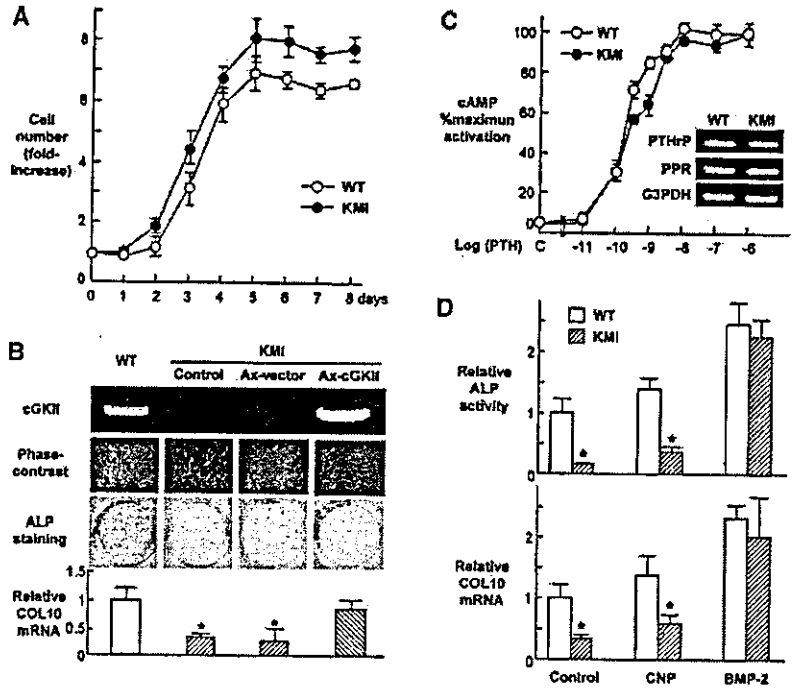

Figure 4. Functions of cultured chondrocytes from wild type and KMI. (*A*) Growth curves of wild-type (WT) and KMI chondrocytes isolated from the growth plate. Data are mean (symbols) ± S.E.M. (error bars) of six dishes/genotype. Lack of significant difference between the genotypes was confirmed in five independent experiments. (*B*) Differentiation of wild-type (WT) and KMI chondrocytes determined by the phase contrast image, ALP staining, and COL10 mRNA level determined by real-time quantitative RT–PCR cultured for 5, 21, and 28 d, respectively. As a rescue experiment, an adenovirus vector carrying the *cGKII* gene (Ax-*cGKII*) or that without the *cGKII* gene (Ax-vector) was introduced into KMI chondrocytes. (*Top* panel) The cGKII mRNA level is shown by RT–PCR. COL10 mRNA levels are mean (bars) ± S.E.M. (error bars) of the relative amount of mRNA compared to that of wild type of six wells/group. (*) $P < 0.05$ vs. wild type. (*C*) PTH/PTHrP signaling determined by the dose-response effects of PTH (10^{-11} to 10^{-6} M) on cAMP accumulation in wild-type (WT) and KMI chondrocytes. Data are mean (symbols) ± S.E.M. (error bars) of the percentages of maximal cAMP activation for six wells/genotype. Lack of significant difference between the genotypes was confirmed in three independent experiments. The PTHrP and PTH/PTHrP receptor (PPR) mRNA levels are shown by RT–PCR as an *inset*. (*D*) Effects of CNP (100 nM) and BMP-2 (100 ng/mL) on the ALP activity and COL10 mRNA level determined by real-time quantitative RT–PCR in the wild-type (WT) and KMI chondrocyte cultures for 21 and 28 d, respectively. Data are mean (bars) ± S.E.M. (error bars) of six wells/group. (*) $P < 0.01$ vs. wild type.

tems. Initially, to know the effects of cGKII and Sox9 on the hypertrophic differentiation of chondrocytes, we examined the COL10 expression in cultured mouse chondrogenic ATDC5 cells (Fig. 5B; Shukunami et al. 1996). In the monolayer culture, the baseline of the COL10 level was low and little altered by the Sox9 transfection; however, in the three-dimensional culture, ATDC5 cells differentiated into hypertrophic chondrocytes with COL10 expression in the presence of insulin, as reported previously (Seki et al. 2003). The Sox9 transfection was confirmed to reduce the COL10 mRNA level, and the cotransfection with cGKII restored it to the control level. In addition, transfection with Sox9 was also confirmed to show an ~10-fold increase in the type II collagen (COL2) mRNA level in human nonchondrogenic hepatoma HuH-7 cells, and cotransfection with cGKII significantly suppressed the Sox9-induced COL2 expression (Fig. 5C). These results suggest a novel function of cGKII as an attenuator of the Sox9 actions: inhibition of hypertrophic differentiation and stimulation of chondrogenic differentiation. We further examined the effects of mutated cGKII: one derived from KMI (cGKII-KMI) and the other lacking the entire kinase domain (cGKII-Δkinase) in the respective cultures (Fig. 5B,C). Neither of the mutant cGKIIs restored the Sox9-inhibited COL10 level nor suppressed the Sox9-induced COL2, implicating that the kinase activity of cGKII was indispensable for the attenuation of the Sox9 function. Hence, we next examined the involvement of phosphorylation of Sox9 in the action of cGKII. The consensus amino acid sequence for phosphorylation by cGKII is RRXS/TX where either S or T is the phosphorylation site (Hofmann 1995), and a single consensus sequence was detected at Ser 181 (S181) in the human Sox9. Immunoblot analysis with a phosphorylation-specific antibody revealed that the cGKII cotransfection stimulated the phosphorylation of transfected Sox9 at S181 in HuH-7 cells (Fig. 5D, top panel). To learn the functional relevance of the Sox9 phosphorylation by cGKII, we generated a phosphorylation-deficient Sox9 vector ($Sox9^{S181A}$) by introducing serine-to-alanine substitutions at S181. The $Sox9^{S181A}$ transfection induced the COL2 expression to a level similar to that of the wild-type Sox9 in HuH-7 cells (Fig. 5D, bottom panel). Interestingly, the cGKII cotransfection decreased the COL2 induction by the $Sox9^{S181A}$ similarly to that by the wild-type Sox9, indicating that the phosphorylation of Sox9 itself is dispensable for the attenuation of the Sox9 function by cGKII.

To clarify the mechanism underlying the attenuation of the Sox9 signaling by cGKII, we examined the subcellular localization of Sox9. Fluorescent images of HeLa cells transfected with the plasmid encoding GFP-Sox9 revealed that Sox9 is predominantly localized in the nucleus, in agreement with previous reports (Fig. 6A; Huang et al. 2001). When cGKII was cotransfected, Sox9 became localized not only in the nucleus, but also in the

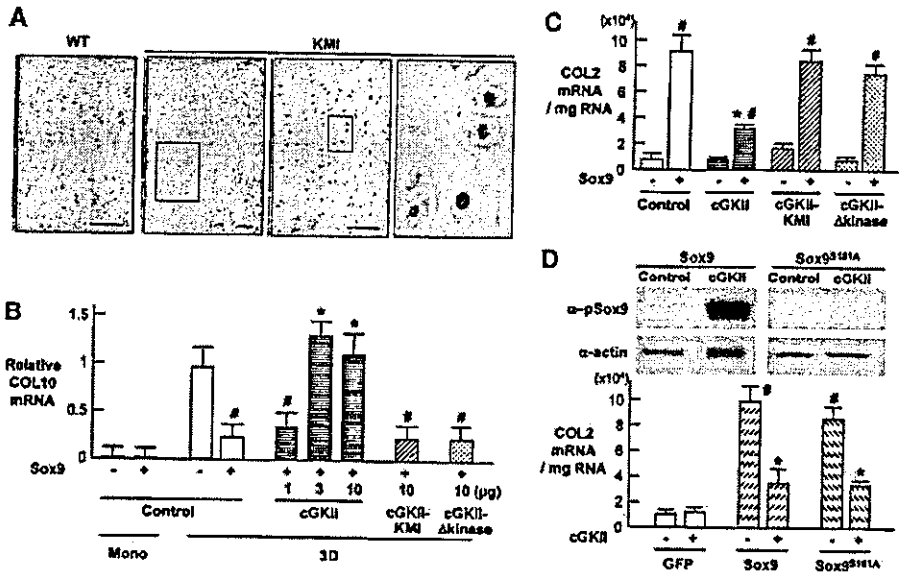

Figure 5. Regulation of Sox9 function and phosphorylation by cGKII. (*A*) Immunohistochemical stainings with an anti-Sox9 antibody in the growth plates of the proximal tibiae of wild type (WT) and KMI at 10 wk of age. *Inset* boxes in the *middle* two panels indicate the regions of the respective *right* panels. Blue, black, red, and green bars indicate layers of proliferative zone, abnormal intermediate zone, hypertrophic zone, and primary spongiosa, respectively. Bar, 50 μm. (*B*) COL10 mRNA levels by the transfection with the plasmid encoding Sox9 determined by real-time quantitative RT–PCR in cultured ATDC5 cells cotransfected with the empty vector (control), the expression vectors of cGKII (1, 3 and 10 μg), cGKII-KMI (10 μg), and cGKII-Δkinase (10 μg) in the monolayer culture (Mono) and three-dimensional alginate beads culture (3D) in the chondrogenic medium with insulin. Data are mean (bars) ± S.E.M. (error bars) of six wells/group. (#) $P < 0.01$, significant inhibition by Sox9. (*) $P < 0.01$, significant stimulation by cGKII. (*C*) Induction of COL2 mRNA by the Sox9 transfection determined by real-time quantitative RT–PCR in cultured HuH-7 cells cotransfected with the empty vector (control), the expression vectors of wild-type cGKII (cGKII), the mutated cGKII lacking exons 4 and 5 (cGKII-KMI), and that lacking the kinase domain (cGKII-Δkinase). Data are mean (bars) ± SEM (error bars) of six wells/group. (#) $P < 0.01$, significant stimulation by Sox9. (*) $P < 0.01$, significant inhibition by cGKII. (*D*, *top*) Immunoblotting with an anti-phosho-Sox9 antibody (α-pSox9) in cultured HuH-7 cells transfected with wild-type Sox9 or phosphorylation-deficient Sox9 ($Sox9^{S181A}$). Blottings with anti-β-actin (α-actin) were used as loading control. (*Bottom*) Induction of COL2 mRNA by the transfection with Sox9 or $Sox9^{S181A}$ determined by real-time quantitative RT–PCR in cultured HuH-7 cells in combination with the cGKII expression vector (+) or the empty vector (–). Data are mean (bars) ± S.E.M. (error bars) of six wells/group. (#) $P < 0.01$, significant stimulation by Sox9. (*) $P < 0.01$, significant inhibition by cGKII.

cytoplasm. Addition of leptomycin B, an inhibitor of CRM-1-dependent nuclear export (Gasca et al. 2002), failed to restore the altered localization of Sox9, suggesting that cGKII attenuated the nuclear entry of Sox9 rather than enhanced its export from the nucleus. As cGKII also altered the subcellular localization of phosphorylation-deficient Sox9 ($Sox9^{S181A}$) in a similar manner, phosphorylation at S181 was shown to be dispensable for this regulatory mechanism. Interestingly, the subcellular localization of Sox5 and Sox6, critical partners of Sox9, was not affected by cGKII (Fig. 6A). The altered subcellular localization of Sox9 was confirmed by an immunoblot analysis: the cGKII cotransfection increased the Sox9 protein level in the cytoplasmic fraction although it decreased that in the nuclear fraction (Fig. 6B). To determine whether or not the attenuated Sox9 signaling by cGKII was attributable to the decreased nuclear entry of Sox9, we fused Sox9 with SV40-derived nuclear localization signal (Sox9-3xNLS), thereby forcing Sox9 to localize in the nucleus. The cGKII cotransfection was unable to keep the Sox9 in the cytoplasm in HeLa cells (Fig. 6C, left panel). In this condition, the inhibitory effect of cGKII on the Sox9-induced COL2 expression was greatly alleviated, indicating that cGKII attenuated the Sox9 function mainly, if not exclusively, by interfering with its nuclear entry (Fig. 6C, right panel). To further examine the change of Sox9 subcellular localization in the KMI chondrocytes, we adenovirally transduced cultured primary chondrocytes from wild-type and KMI growth plates with GFP-Sox9. Treatment with the cGMP analog 8-bromo-cGMP inhibited nuclear entry of Sox9 in wild-type cells, whereas it did not in KMI cells. CNP, a putative upstream molecule of cGKII, showed a similar effect on the Sox9 subcellular localization in wild-type cells, but not in KMI cells (Fig. 6D). Finally, we examined the effects of the silencing of Sox9 through RNA interference (RNAi) on the cultured growth plate chondrocytes from KMI (Fig. 6E). The impaired differentiation of KMI chondrocytes determined by the ALP staining and the COL10 mRNA level was reversed by the retrovirus-mediated introduction of Sox9 RNAi. Taken together, these results demonstrate that

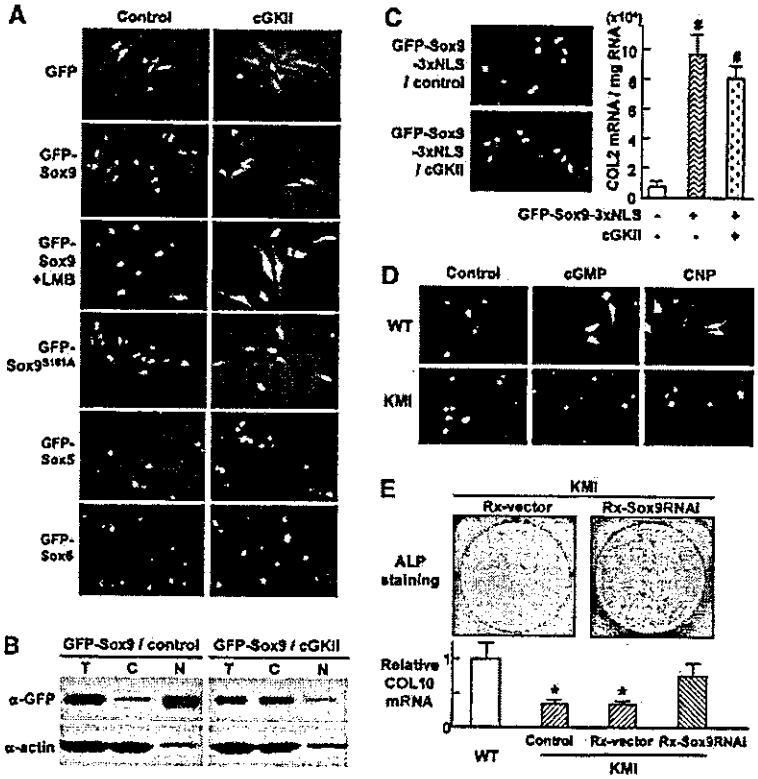

Figure 6. Regulation of Sox9 function and subcellular localization by cGKII. (*A*) Fluorescent images of HeLa cells cotransfected with cGKII and Sox9, Sox5, or Sox6. Cells were transfected with plasmids encoding GFP, GFP-tagged Sox9 (GFP-Sox9) in the presence and absence of a nuclear export inhibitor leptomycin (LMB; 2 ng/mL), and GFP-Sox9^{S181A}, GFP-Sox5, and GFP-Sox6 in combination with the cGKII expression vector or the empty vector (control). (*B*) Subcellular localization of Sox9 in HeLa cells by immunoblotting. GFP-Sox9 was cotransfected with the cGKII expression vector or the empty vector (control). The Sox9 protein levels in the total cell lysate (T), cytoplasmic fraction (C), and nuclear fraction (N) were determined by immunoblotting with an anti-GFP antibody (α-GFP). Blottings with anti-β-actin (α-actin) were used as loading controls. (*C*, *left*) Fluorescent images of HeLa cells transfected with the nuclear-localizing Sox9 vector. Three tandem repeats of SV40-derived nuclear localizing signal (NLS) were introduced into the GFP-Sox9 vector (GFP-Sox9-3xNLS). Cells were transfected with the GFP-Sox9-3xNLS in combination with the cGKII expressing vector or the empty vector (control). (*Right*) Induction of COL2 mRNA by the GFP-Sox9-3xNLS transfection determined by real-time quantitative RT–PCR in cultured HuH-7 cells cotransfected with the cGKII expression vector (+) or the empty vector (−). Data are mean (bars) ± S.E.M. (error bars) of six wells/group. (#) $P < 0.01$, significant stimulation by GFP-Sox9-3xNLS. (*D*) Fluorescent images of wild-type (WT) and KMI growth plate chondrocytes transduced with GFP-Sox9 adenovirus vector. Primary chondrocytes were cultured in the presence and absence of 8-Bromo-cGMP (100 μM) or CNP (100 nM). (*E*) Effects of the silencing of Sox9 through RNAi on the ALP staining and the COL10 mRNA level determined by real-time quantitative RT–PCR in the KMI chondrocyte culture for 21 and 28 d, respectively. The Sox9 RNAi was introduced into KMI chondrocytes using an retrovirus vector carrying the Sox9 RNAi gene (Rx-Sox9RNAi). Retrovirus vector without the Sox9 RNAi gene (Rx-vector) was used as control. Data are mean (bars) ± S.E.M. (error bars) of six wells/group. (*) $P < 0.01$ vs. wild type.

the cGKII dysfunction in KMI impaired the hypertrophic differentiation of chondrocytes through enhancement of the Sox9 signaling.

Discussion

Although postproliferative chondrocytes immediately undergo hypertrophic differentiation during endochondral ossification, little has been known about the molecular mechanism that couples the cessation of proliferation and the start of hypertrophy. The present study for the first time identified a novel role of cGKII as a molecular switch for the coupling. The study began with the identification of a mutation in the *cGKII* gene causing the longitudinal growth retardation of a rat dwarf model, KMI. Analyses of the growth plate and the bone fracture callus of KMI revealed that the cessation of proliferation and the start of hypertrophic differentiation of chondrocytes were dissociated. Cultures of KMI chondrocytes confirmed that the cGKII dysfunction impairs the synchronized switching from proliferation to hypertrophic differentiation. This KMI chondrocyte abnormality may be due to the sustained activity of Sox9, as cGKII was shown to function as an attenuator of Sox9 mainly by inhibiting its nuclear entry.

Physiological function of cGKII

In mammalian cells, at least three receptors for cGMP are present, that is, cGMP-regulated PDEs, cyclic nucleotide-gated cation channels, and cGKs (Ruth 1999). Mammalian cGKs exist as two isoforms, cGKI and cGKII (Hofmann et al. 2000). Whereas the cGKI is expressed at high levels in all types of smooth muscle, platelets, and cerebellar cells, cGKII is expressed in the intestinal mucosa, juxtaglomerular cells of the kidney, and chondrocytes (Pfeifer et al. 1996). The widespread expression of cGKs is mirrored by the diversity of their functions, which establish these enzymes as major mediators of the cGMP signaling cascade. Studies on the ablation of the genes disclosed the pivotal tasks of these enzymes under in vivo conditions (Pfeifer et al. 1996, 1998). *cGKII*-deficient (*cGKII*$^{-/-}$) mice were reported to develop dwarfism postnatally, which was caused by a severe defect in en-

dochondral ossification at the growth plates (Pfeifer et al. 1996). Although the phenotypes were quite similar to those of KMI, the abnormal population of chondrocytes in the *cGKII*$^{-/-}$ growth plate was though to constitute a hypertrophic zone with patches of nonhypertrophic cells intermingled with hypertrophic chondrocytes. Our more detailed histological examination of the KMI growth plate clearly showed that these cells were postmitotic but nonhypertrophic chondrocytes. Further examinations of the *cGKII*$^{-/-}$ growth plate would probably reveal similar findings confirming the unique role of cGKII in the coupling of chondrocyte proliferation and differentiation.

cGKII and CNP signaling

CNP is a positive regulator of endochondral ossification through the intracellular accumulation of cGMP, which activates different signaling mediators such as cyclic nucleotide phosphodiesterases, cGMP-regulated ion channels, and cGKs (Fowkes and McArdle 2000). Among them, cGKII is reported to play a critical role in the CNP action on endochondral ossification, because targeted expression of CNP in the growth plate chondrocytes failed to rescue the skeletal defect of *cGKII*$^{-/-}$ mice (Miyazawa et al. 2002). This notion was supported by the present findings that CNP neither reverses the impaired differentiation (Fig. 4D) nor inhibits the Sox9 nuclear entry (Fig. 6D) in cultured KMI chondrocytes. However, there is a marked difference between *CNP*$^{-/-}$ and *cGKII*$^{-/-}$ mice in the histology of the growth plate (Pfeifer et al. 1996; Chusho et al. 2001): the growth plate of the former is reduced in height with the chondrocytes arranged in a regular columnar array, whereas that of the latter is increased in height. This may indicate the involvement of other signaling pathway(s) in the CNP-mediated endochondral ossification. In fact, a recent report showed that targeted overexpression of CNP in chondrocytes prevented the shortening of achondroplastic bones through inhibition of the mitogen-activated protein (MAP) kinase pathway of activated fibroblast growth factor receptor 3 signaling in the growth plate (Yasoda et al. 2004). In addition, the possibility of the involvement of cGKI cannot be ruled out, although no skeletal abnormality has been reported in *cGKI*$^{-/-}$ mice (Pfeifer et al. 1998). It would be helpful to investigate whether mice doubly deficient for *cGKI* and *cGKII* mimic the phenotype of *CNP*$^{-/-}$ mice.

cGKII and PTH/PTHrP signaling

Targeted expression of a constitutively active PTH/PTHrP receptor delays endochondral ossification through ligand-independent constitutive cAMP accumulation and the subsequent cAMP-dependent protein kinase (cAK) activation (Schipani et al. 1997). The growth plate histology of the transgenic mice expressing a constitutively active PTH/PTHrP receptor is characterized by the irregular and broadened zone lacking the COL10 expression, which is similar to that of KMI and *cGKII*$^{-/-}$ mice. In the present study, however, neither the expression levels of PTHrP and PTH/PTHrP receptor nor the cAMP accumulation by PTH stimulation was enhanced in the cultured KMI chondrocytes. It is therefore speculated that the cGKII and PTH/PTHrP/cAK signaling pathways independently coordinate to control the rate of chondrocytic differentiation as an accelerator and a decelerator, respectively.

Regulation of Sox9 actions by cGKII

In addition to its essential roles in early mesenchymal condensation and development of premature chondrocytes, Sox9 is reported to prevent hypertrophic differentiation of chondrocytes (de Crombrugghe et al. 2001; Akiyama et al. 2002). Although the present findings demonstrated that cGKII maintains the hypertrophy by attenuating the Sox9 activity, the molecular mechanism remains to be clarified in more detail. The fact that cGKII lacking the kinase activity did not suppress the Sox9 function suggests that phosphorylation by cGKII is required for the regulation of Sox9 activity. Although cGKII enhanced the phosphorylation of Sox9 at S181, which has been known to be a phosphorylation target for PKA signaling (Huang et al. 2000), the attenuation of Sox9 by cGKII was not dependent on the phosphorylation at this site (Fig. 5D). Along with S181, Ser 64 (S64) is also known to be a phosphorylation target for PKA (Huang et al. 2000); however, this site does not contain the consensus sequence for phosphorylation by cGKII (RRXS/TX). In addition, cGKII suppressed the COL2 induction in cultured HuH-7 cells transfected with a phosphorylation-deficient Sox9 vector at this site ($Sox9^{S64A}$) as with the wild-type Sox9 or $Sox9^{S181A}$ (data not shown), indicating that the direct phosphorylation of Sox9 is dispensable for its attenuation by cGKII. Several lines of evidence indicated that transcriptional factors of the Sox family are regulated by subcellular distribution (Sudbeck and Scherer 1997; Harley et al. 2003). The present findings also indicate that cGKII attenuates the Sox9 function at least in part by inhibiting its nuclear entry. Because this cGKII effect was seen in cells transfected with the phosphorylation-deficient Sox9, the phosphorylation and the nuclear entry of Sox9 were independent, although both were affected by cGKII. Hence, there seem to be other phosphorylation target molecules that mediate cGKII signaling. Sox genes including Sox9 require partner molecules that enhance or suppress transcriptional activities. For example, Sox5 and Sox6 cooperatively work with Sox9 and activate several cartilage matrix genes (Lefebvre and deCrombugghe 1998); however, our computer search found no amino acid sequence in Sox5 or Sox6 for a cGKII phosphorylation site like S181 in Sox9. Furthermore, our results revealed that their subcellular localizations were not altered by cGKII (Fig. 6A), suggesting that it is unlikely that Sox5 and Sox6 are the direct target of cGKII. It was recently revealed that the dimerization of Sox9 is critical for its several target genes. Sox9 contains a dimerization domain and binds

cooperatively as a dimer in the presence of the DNA enhancer element in genes involved in chondrocyte differentiation, such as COL9, COL11, and CD-Rap (Sock et al. 2003). Because in vitro-transcripted Sox9 was unable to form a DNA-dependent dimer (Lefebvre et al. 1998), there must be cofactor(s) that mediate the dimerization of Sox9. Although phosphorylation of these partner molecules remains to be resolved, one of these molecules might be a direct or indirect phosphorylational target of cGKII.

cGKII, a molecular switch from proliferation to hypertrophic differentiation of chondrocytes, could be a novel therapeutic target for disorders of skeletal growth and regeneration. Because cGKII is an intracellular kinase, we are planning to apply the gene transfer system that we are now intensively working on (Itaka et al. 2002) for bone regenerative medicine. Otherwise, a small compound that modulates cGKII activity in vivo would be a good candidate for a new therapeutic drug.

Materials and methods

Genetic mapping

Heterozygous (BN × KMI-*mri/mri*) F1 rats were backcrossed to KMI-*mri/mri* homozygous rats to obtain backcross progeny (241 homozygotes among 475 backcross progeny). Animals were genotyped with SSLP markers (Rat Genome Database, http://rgd.mcw.edu). The segregation patterns of the markers were analyzed with the Map Manager computer program. The rat–mouse–human comparative map was constructed based on the data obtained from the following databases: RatMap (http://ratmap.gen.gu.se), Mouse Genome Informatics (http://www.informatics.jax.org), and University of California at Santa Cruz Genome Browser (http://genome.ucsc.edu).

Positional candidate cloning of the mri *locus*

Total RNA from rat intestine was prepared and subjected to RT–PCR using specific primers to amplify overlapping products that cover the coding region of the rat *cGKII* gene. Genomic DNA was isolated from rat liver, and interexon PCR was carried out with primers as follows: 5′-CTTATCACAGACGCCCTGAATAAGAAC-3′ and 5′-CACTTCCAAGCAGTCAATAATCTTGGT-3′. The amplified pruducts were sequenced using ABI PRISM 310 Genetic Analyzer (Applied Biosystems).

Animals were genotyped with primers as follows: common forward, 5′-TGTATTTTCCCGTCCGACAC-3′; wild-type reverse, 5′-TCCTTCGATGCCACCGTAAT-3′; and KMI reverse, 5′-CAGAGTACGCTAGGTTCCAAGG-3′.

In vitro kinase assay

Wild-type and KMI brain extracts (40 µg) were prepared using T-PER (Pierce). Kinase activity was determined by the phosphorylation of biotinylated substrate peptide (250 µM, Biotynyl-RKISASEFDRPLR-OH, Bachem) in the presence of PKI (2 µM, Sigma) and 8-bromo-cGMP (100 µM) for 30 min at 30°C using the AUSA Universal Protein Kinase Assay Kit (TRANSBIO).

Histological analysis

Tissues were fixed in 4% paraformaldehyde and decalcified in 10% EDTA, if necessary, then embedded in paraffin and cut into 6-µm sections. Hematoxylin eosin (HE) staining and von Kossa staining were done according to the standard procedure. For enzyme histochemistry, ALP was visualized using X-phosphate and NBT (Roche). For immunohistochemistry, sections were incubated with primary antibody at 4°C overnight. Primary antibodies were purchased from Santa Cruz Biotechnology. Signal was detected with HRP-conjugated secondary antibody. For fluorescent visualization, a secondary antibody conjugated with Alexa 488 (Molecular Probes) was used.

In vivo BrdU labeling

Animals were injected intraperitoneally with BrdU (Sigma), 25 µg per gram body weight 2 h prior to sacrifice. Incorporated BrdU was detected using a BrdU immunostaining kit (Roche).

Fracture model

A fracture was generated on the mid-part of the tibiae of 10-week-old animals (n = 10/group). Animals were sacrificed 2 wk after the surgery. Fracture callus was quantitated as described (Shimoaka et al. 2004).

Analysis of growth plate chondrocytes

Growth plate chondrocytes were isolated from the tibiae of 4-week-old animals as described (Klaus et al. 1991). Cells were cultured in Dubecco's Modified Eagle's Medium (DMEM) supplemented with 10% fetal bovine serum (FBS). For cellular proliferation assay, 1×10^5 cells were plated on a 6-cm dish and counted after designated periods. To assess differentiation, cells were incubated for a designated period with hBMP-2 (100 ng/mL) and CNP (100 nM) when needed. They were stained for ALP, and ALP activity was quantitated as described (Shimoaka et al. 2004). RNA was isolated and subjected to semiquantitative RT–PCR analysis. Primer information will be provided upon request.

Plasmids and viral vectors

cDNA of rat cGKII (nucleotides 48–2333) was ligated into pcDNA4HisA (Invitrogen). A PCR-amplified fragment (nucleotides 48–1403) was used to construct the cGKII-Δkinase vector. Full-length human Sox5, Sox6, and Sox9 were ligated into pEGFPC1 (Clontech) to generate GFP-tagged plasmids. To create amino acid change (S181A and S64A), GFP-Sox9 plasmid was subjected to site-directed mutagenesis using the inverse PCR technique. To construct nuclear-localizing GFP-Sox9 vector (Sox9-3xNLS), a three-tandem repeat of SV40-derived nuclear localizing signal was ligated into pEGFPC1. All constructs were verified by sequencing. cGKII and GFP-Sox9 adenovirus vectors were constructed using the Adeno-X Expression System (BD Biosciences), according to the manufacturer's protocol. RNAi sequence was designed for the rat *Sox9* gene (nucleotides 190–219, AB073720.1) as described (Kawasaki and Taira 2003) and ligated into piGENEtRNA vector (iGENE Therapeutics). RNAi sequence combined with promotor was then inserted into pMx vector (Kitamura 1998), and retroviral vector was generated using plat-E cells (Morita et al. 2000).

Cell culture and transient transfection

HuH-7 and HeLa were cultured in DMEM supplemented with 10% FBS. ATDC5 was maintained as described (Shukunami et al. 1996). For transient transfection, a total of 1 µg plasmid DNA was transfected using FuGENE6 (Roche). In cotransfection, all

plasmids were added in an equal ratio. 8-bromo-cGMP (100 µM, BioMol) was added 4 h after transfection. Total RNA was isolated 72 h after transfection and subjected to real-time PCR analysis. For fluorescent detection, HeLa cells were transiently transfected and fluorescent images were taken 24 h after transfection. Cells were incubated with 2.5 ng/mL leptomycin B (Sigma) for the last 3 h when required. For the differentiation assay, ATDC5 cells were transiently cotransfected with Sox9 vector (3 µg) and a designated amount of cGKII vector. Two days after transfection, a three-dimensional alginate beads culture was performed as described (Seki et al. 2003) in the presence of 8-bromo-cGMP (100 µM) and ITS supplement (Sigma). RNA was isolated 7 d after transfection and subjected to real-time PCR analysis.

Western blotting

Samples were prepared using M-PER (Pierce) or NE-PER (Pierce) supplemented with Na_3Vo_4 (2 mM), NaF (10 mM), and aprotinin (10 µg/mL) following the manufacturer's protocol. An equal amount (20 µg) of protein was subjected to SDS-PAGE, and transferred onto PVDF membranes. Anti-EGFP antibody (Clontech) and anti-Sox9 (pS^{181}) phosphospecific antibody (BioSource) were used. The membrane was incubated with HRP-conjugated secondary antibody (Promega). Immunoreactive proteins were visualized by ECL (Amersham).

PTH-induced cAMP accumulation

Cells were preincubated with 8-bromo-cGMP (100 µM) for 30 min, then challenged with increasing concentrations of PTH (Sigma) and incubated at 37°C for 30 min in the presence of IBMX (2 mM). Intercellular cAMP was measured using the cAMP Biotrack EIA system (Amersham) following the manufacturer's protocol.

Statistical analysis

Means of groups were compared by ANOVA, and significance of differences was determined by post-hoc testing with Bonferroni's method.

Acknowledgments

We thank Drs. Benoit de Crombrugghe, Sakae Tanaka, Yasuo Terauchi, and Takashi Kadowaki for critical discussions. We also thank Reiko Yamaguchi, Mizue Ikeuchi, and Misako Namae for their excellent technical help. This work was supported by Grants-in-Aid for Scientific Research from the Japanese Ministry of Education, Culture, Sports, Science and Technology (#14657359 and #15591566).

References

Akiyama, H., Chaboissier, M.C., Martin, J.F., Schedl, A., and de Crombrugghe, B. 2002. The transcription factor Sox9 has essential roles in successive steps of the chondrocyte differentiation pathway and is required for expression of Sox5 and Sox6. *Genes & Dev.* **16:** 2813–2828.

Chung, U. and Kronenberg, H. 2000. Role of parathyroid hormone-related protein and indian hedgehog in skeletal development. In *Skeletal growth factors* (ed. C. Canalis), pp. 355–364. Lippincott Willams & Wilkins, Philadelphia.

Chusho, H., Tamura, N., Ogawa, Y., Yasoda, A., Suda, M., Miyazawa, T., Nakamura, K., Nakao, K., Kurihara, T., Komatsu, Y., et al. 2001. Dwarfism and early death in mice lacking C-type natriuretic peptide. *Proc. Natl. Acad. Sci.* **98:** 4016–4021.

Daluiski, A., Engstrand, T., Bahamonde, M.E., Gamer, L.W., Agius, E., Stevenson, S.L., Cox, K., Rosen, V., and Lyons, K.M. 2001. Bone morphogenetic protein-3 is a negative regulator of bone density. *Nat. Genet.* **27:** 84–88.

de Crombrugghe, B., Lefebvre, V., and Nakashima, K. 2001. Regulatory mechanisms in the pathways of cartilage and bone formation. *Curr. Opin. Cell Biol.* **13:** 721–727.

Fowkes, R.C. and McArdle, C.A. 2000. C-type natriuretic peptide: An important neuroendocrine regulator? *Trends Endocrinol. Metab.* **11:** 333–338.

Gasca, S., Canizares, J., De Santa Barbara, P., Mejean, C., Poulat, F., Berta, P., and Boizet-Bonhoure, B. 2002. A nuclear export signal within the high mobility group domain regulates the nucleocytoplasmic translocation of SOX9 during sexual determination. *Proc. Natl. Acad. Sci.* **99:** 11199–11204.

Harley, V.R., Clarkson, M.J., and Argentaro, A. 2003. The molecular action and regulation of the testis-determining factors, SRY (sex-determining region on the Y chromosome) and SOX9 [SRY-related high-mobility group (HMG) box 9]. *Endocr. Rev.* **24:** 466–487.

Hofmann, F. 1995. cGMP-dependent protein kinase (vertebrates). In *The protein kinase factsbook* (eds. G. Hardie and S. Hanks), pp. 73–76. Academic Press, San Diego.

Hofmann, F., Ammendola, A., and Schlossmann, J. 2000. Rising behind NO: cGMP-dependent protein kinases. *J. Cell Sci.* **113:** 1671–1676.

Huang, W., Zhou, X., Lefebvre, V., and de Crombrugghe, B. 2000. Phosphorylation of SOX9 by cyclic AMP-dependent protein kinase A enhances SOX9's ability to transactivate a Col2a1 chondrocyte-specific enhancer. *Mol. Cell Biol.* **20:** 4149–4158.

Huang, W., Chung, U.I., Kronenberg, H.M., and de Crombrugghe, B. 2001. The chondrogenic transcription factor Sox9 is a target of signaling by the parathyroid hormone-related peptide in the growth plate of endochondral bones. *Proc. Natl. Acad. Sci.* **98:** 160–165.

Itaka, K., Harada, A., Nakamura, K., Kawaguchi, H., and Kataoka, K. 2002. Evaluation by fluorescence resonance energy transfer of the stability of nonviral gene delivery vectors under physiological conditions. *Biomacromolecules* **3:** 841–845.

Kawasaki, H. and Taira, K. 2003. Short hairpin type of dsRNAs that are controlled by tRNA(Val) promoter significantly induce RNAi-mediated gene silencing in the cytoplasm of human cells. *Nucleic Acids Res.* **31:** 700–707.

Kitamura, T. 1998. New experimental approaches in retrovirus-mediated expression screening. *Int. J. Hematol.* **67:** 351–359.

Klaus, G., Merke, J., Eing, H., Hugel, U., Milde, P., Reichel, H., Ritz, E., and Mehls, O. 1991. 1,25(OH)2D3 receptor regulation and 1,25(OH)2D3 effects in primary cultures of growth cartilage cells of the rat. *Calcif. Tissue Int.* **49:** 340–348.

Kronenberg, H.M. 2003. Developmental regulation of the growth plate. *Nature* **423:** 332–336.

Lefebvre, V., Li, P., and de Crombrugghe, B. 1998. A new long form of Sox5 (L-Sox5), Sox6 and Sox9 are coexpressed in chondrogenesis and cooperatively activate the type II collagen gene. *EMBO J.* **17:** 5718–5733.

Miyazawa, T., Ogawa, Y., Chusho, H., Yasoda, A., Tamura, N., Komatsu, Y., Pfeifer, A., Hofmann, F., and Nakao, K. 2002. Cyclic GMP-dependent protein kinase II plays a critical role in C-type natriuretic peptide-mediated endochondral ossification. *Endocrinology* **143:** 3604–3610.

Morita, S., Kojima, T., and Kitamura, T. 2000. Plat-E: An effi-

cient and stable system for transient packaging of retroviruses. *Gene Ther.* 7: 1063–1066.

Pfeifer, A., Aszodi, A., Seidler, U., Ruth, P., Hofmann, F., and Fassler, R. 1996. Intestinal secretory defects and dwarfism in mice lacking cGMP-dependent protein kinase II. *Science* 274: 2082–2086.

Pfeifer, A., Klatt, P., Massberg, S., Ny, L., Sausbier, M., Hirneiss, C., Wang, G.X., Korth, M., Aszodi, A., Andersson, K.E., et al. 1998. Defective smooth muscle regulation in cGMP kinase I-deficient mice. *EMBO J.* 17: 3045–3041.

Ruth, P. 1999. Cyclic GMP-dependent protein kinases: Understanding in vivo functions by gene targeting. *Pharmacol. Ther.* 82: 355–372.

Schipani, E., Lanske, B., Hunzelman, J., Luz, A., Kovacs, C.S., Lee, K., Pirro, A., Kronenberg, H.M., and Juppner, H. 1997. Targeted expression of constitutively active receptors for parathyroid hormone and parathyroid hormone-related peptide delays endochondral bone formation and rescues mice that lack parathyroid hormone-related peptide. *Proc. Natl. Acad. Sci.* 94: 13689–13694.

Seki, K., Fujimori, T., Savagner, P., Hata, A., Aikawa, T., Ogata, N., Nabeshima, Y., and Kaechoong, L. 2003. Mouse Snail family transcription repressors regulate chondrocyte, extracellular matrix, type II collagen, and aggrecan. *J. Biol. Chem.* 278: 41862–41870.

Serizawa, N. 1993. Initial characterization of a new miniature animal model in the rat: Studies on anatomy, pituitary hormones and GH mRNA in miniature rat Ishikawa. *Nippon Naibunpi Gakkai Zasshi* 69: 33–45.

Shimoaka, T., Kamekura, S., Chikuda, H., Hoshi, K., Chung, U.I., Akune, T., Maruyama, Z., Komori, T., Matsumoto, M., Ogawa, W., et al. 2004. Impairment of bone healing by insulin receptor substrate-1 deficiency. *J. Biol. Chem.* 279: 15314–15322.

Shukunami, C., Shigeno, C., Atsumi, T., Ishizeki, K., Suzuki, F., and Hiraki, Y. 1996. Chondrogenic differentiation of clonal mouse embryonic cell line ATDC5 in vitro: Differentiation-dependent gene expression of parathyroid hormone (PTH)/PTH-related peptide receptor. *J. Cell Biol.* 133: 457–468.

Sock, E., Pagon, R.A., Keymolen, K., Lissens, W., Wegner, M., and Scherer, G. 2003. Loss of DNA-dependent dimerization of the transcription factor SOX9 as a cause for campomelic dysplasia. *Hum. Mol. Genet.* 12: 1439–1447.

Sorrentino, V., Pepperkok, R., Davis, R.L., Ansorge, W., and Philipson, L. 1990. Cell proliferation inhibited by MyoD1 independently of myogenic differentiation. *Nature* 345: 813–815.

Stewart, M.C., Kadlcek, R.M., Robbins, P.D., MacLeod, J.N., and Ballock, R.T. 2004. Expression and activity of the CDK inhibitor p57Kip2 in chondrocytes undergoing hypertrophic differentiation. *J. Bone Miner. Res.* 19: 123–132.

Sudbeck, P. and Scherer, G. 1997. Two independent nuclear localization signals are present in the DNA-binding high-mobility group domains of SRY and SOX9. *J. Biol. Chem.* 272: 27848–27852.

Tao, H. and Umek, R.M. 2000. C/EBPα is required to maintain postmitotic growth arrest in adipocytes. *DNA Cell Biol.* 19: 9–18.

Umek, R.M., Friedman, A.D., and McKnight, S.L. 1991. CCAAT-enhancer binding protein: A component of a differentiation switch. *Science* 251: 288–292.

Yan, Y., Frisen, J., Lee, M.H., Massague, J., and Barbacid, M. 1997. Ablation of the CDK inhibitor p57Kip2 results in increased apoptosis and delayed differentiation during mouse development. *Genes & Dev.* 11: 973–983.

Yasoda, A., Komatsu, Y., Chusho, H., Miyazawa, T., Ozasa, A., Miura, M., Kurihara, T., Rogi, T., Tanaka, S., Suda, M., et al. 2004. Overexpression of CNP in chondrocytes rescues achondroplasia through a MAPK-dependent pathway. *Nat. Med.* 10: 80–86.

J|A|C|S
COMMUNICATIONS

Published on Web 09/30/2004

Supramolecular Nanocarrier of siRNA from PEG-Based Block Catiomer Carrying Diamine Side Chain with Distinctive pK_a Directed To Enhance Intracellular Gene Silencing

Keiji Itaka,[†,‡] Naoki Kanayama,[†] Nobuhiro Nishiyama,[†] Woo-Dong Jang,[†] Yuichi Yamasaki,[†] Kozo Nakamura,[‡] Hiroshi Kawaguchi,[‡] and Kazunori Kataoka*[,†]

Department of Materials Science and Engineering, Graduate School of Engineering, and Department of Orthopaedic Surgery, Faculty of Medicine, University of Tokyo, 7-3-1 Hongo, Bunkyo-ku, Tokyo 113-8656, Japan

Received May 14, 2004; E-mail: kataoka@bmw.t.u-tokyo.ac.jp

The short double-stranded RNA species, called short interference RNA (siRNA), can be used to silence the gene expression in a sequence-specific manner in a process that is known as RNA interference (RNAi).[1] It has become a useful method for the analysis of gene functions and holds the significant possibility of therapeutic application. However, to promote an efficient gene knockdown, especially in an in vivo situation, two substantial issues must be considered: tolerability under physiological conditions and enhanced cellular uptake. Thus, the development of effective siRNA delivery systems is required.

Recently, a new delivery system of plasmid DNA and oligonucleotides has been developed, based on the micellar assembly of the poly-ion complex (PIC) of these compounds with block copolymers consisting of poly(ethylene glycol) (PEG) and polycation segments, leading to the self-assembled structure with a core−shell architecture (PIC micelles).[2] Their excellent properties for in vivo DNA delivery have been confirmed so far:[3] a diameter around 100 nm with a PEG palisade which enables complexes to avoid recognition by reticuloendothelial systems, increased nuclease resistance, increased tolerance under physiological conditions, and the excellent gene expression in a serum-containing medium.[4]

We now describe the structural design of a novel block catiomer-based PIC particularly available for siRNA delivery. PEG−poly-(3-[(3-aminopropyl)amino]propylaspartamide (PEG-DPT; PEG, 12 000 g/mol, polymerization degree of DPT segment, 68), carrying a diamine side chain with distinctive pK_a, was newly synthesized by a side-chain aminolysis reaction of PEG−poly(β-benzyl-L-aspartate) block copolymer (PEG-PBLA) with dipropylene triamine (DPT) (Figure 1A and Figure S1 in the Supporting Information). A model compound of a DPT unit, *tert*-butoxycarbonyl-β-*N*-3-(3-aminopropyl)aminopropylamido-α-*N*-propyl-(L)-aspartamide (Boc-Asp(DPT)-Pr), was also synthesized (see Supporting Information) to determine the pK_a values of the amino groups.

Boc-Asp(DPT)-Pr clearly gave a two-stage pH−α curve (Figure 1B), from which the pK_a values of the primary and secondary amino groups were determined to be 9.9 and 6.4, respectively. Amino groups in the PIC of polyamine with polynucleotides including siRNA generally undergo facilitated protonation due to the zipper effect or the neighboring group effect during the complexation process, hampering the proton buffering or the proton sponge capacity. The unique feature of PEG-DPT is the regulated location of primary and secondary amino groups in the side chain: the former, with higher pK_a, settles at the distal end of the side chain to participate in the ion complex formation with phosphate groups in siRNA molecule, whereas the latter, with lower pK_a, located closer to the polymer backbone, is expected to leave a substantial

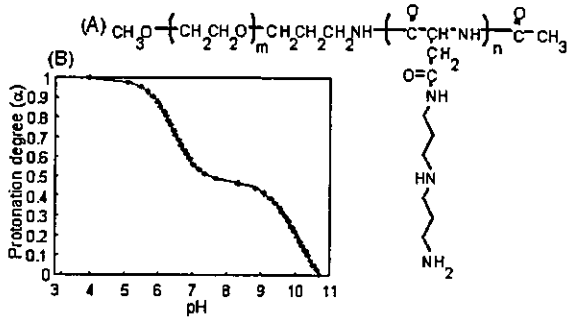

Figure 1. (A) Chemical structure of PEG-DPT. (B) Change in protonation degree (α) with pH for Boc-Asp(DPT)-Pr.

fraction of unprotonated form even in the complex, presumably due to the lower protonation power and the spatial restriction, directing to the enhanced intracellular activity of siRNA through the buffering capacity in the endosomal compartment.

The formation of the siRNA complex with the PEG-DPT was confirmed by polyacrylamide gel electrophoresis (PAGE) and the ethidium bromide (EtBr) exclusion assay (see Figure S2 in the Supporting Information). Note that intercalators such as EtBr bind the double-stranded (ds) RNA in the same fashion as dsDNA.[5] The free siRNA disappeared at the N/P ratio (= [total amines in cationic segment]/[siRNA phosphates]) >2, in line with a substantial fluorescence quenching of EtBr at N/P ≥ 2 due to the inaccessibility of EtBr to the complexed siRNA with PEG-DPT. Furthermore, the EtBr assay highlights the distinctive role of primary and secondary amino groups of the side chain in the complex. The PIC of the double-stranded oligo DNA, composed of sequences similar to the GL3 targeting siRNA, with PEG−poly(3-dimethylamino)propyl aspartamide (PEG-DMAPA; pK_a ≈ 7.9, see Figure S3 for chemical structure), revealed a lower degree of EtBr quenching compared to the PEG-DPT/ds-oligo DNA PIC, even in the region of excess N/P ratios (see Figure S4), suggesting that the presence of unprotonated amino groups in the former may hamper the tight association. PEG−poly(L-lysine) (PEG-PLL; pK_a ≈ 9.37, see Figure S3 for chemical structure) induced EtBr quenching as significantly as PEG-DPT upon complexation with the ds-oligo DNA, yet the quenching leveled off at the stoichiometric N/P ratio (N/P = 1.0) (Figure S4). This is in sharp contrast with the PEG-DPT/ds-oligo DNA complex, which showed leveling-off behavior of EtBr quenching at N/P ≈ 2.0, suggesting that secondary amines with the lower pK_a may be excluded from the ion complexation with oligonucleotides.

These distinctive features of the PEG-DPT, PEG-DMAPA, and PEG-PLL complexes indeed correlated with their gene knockdown abilities. For this evaluation, the GL3 luciferase gene was targeted

[†] Department of Materials Science and Engineering.
[‡] Department of Orthopaedic Surgery.

10.1021/ja047174r CCC: $27.50

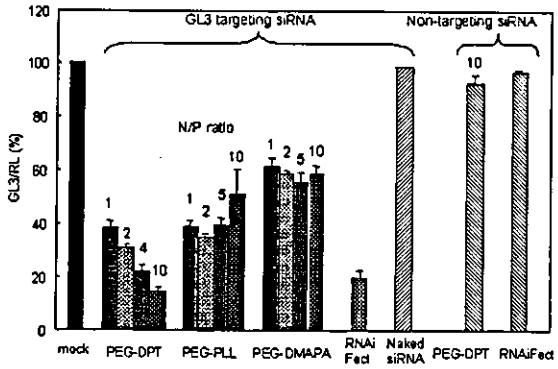

Figure 2. GL3 luciferase gene knockdown ($n = 4$; ±SD).

after transfecting two kinds of luciferase pDNAs (pGL3 and pRL; Promega) to HuH-7 cells. The expression ratio of GL3/RL was used as the knockdown marker.

Each complex system showed a sufficient knockdown of the GL3 luciferase, while neither the naked siRNA nor the nontargeting siRNA showed any knockdown (Figure 2). Thus, these results should be recognized as the veritable RNAi by the GL3-targeting siRNA delivered into the cytoplasm. Notably, the gene knockdown abilities of the siRNA/PEG-DPT complex were superior to those of the other two complexes, especially at higher N/P ratios. At N/P = 10, it showed more than an 80% knockdown, which exceeded the commercial RNAiFect. The cell viability evaluated by MTT assay was more than 75% of the mock cells, even after co-incubation with siRNA/PEG-DPT with N/P ≥ 10 (see Figure S5), suggesting the toxic effect to be eliminated. The siRNA/PEG-DMAPA complexes showed knockdown abilities to a lesser extent. Apparently, the loosely associated nature of siRNA, suggested by the EtBr exclusion assay, is unfavorable for facilitating an effective intracellular delivery of intact siRNA. PEG-PLL showed a considerable knockdown ability in the low N/P region, yet no particular enhancement with the increase in the N/P ratios. High efficacy of PEG-DPT may be characterized by the existence of additional secondary amines with a lower pK_a to promote the internalization of the siRNA molecules into the cytoplasm through buffering of the endosomal cavity, as is the case with the polyethylenimine-based polyplex that shows an enhanced tranfection efficiency at the higher N/P ratios.[6]

A serum incubation study was then performed to evaluate the complex stability under physiological conditions by incubating the complexes in 50% serum at 37 °C prior to transfection. The siRNA/PEG-DPT complexes showed comparable abilities of gene knockdown, even after co-incubation with serum for 30 min (Figure 3A). In contrast, the lipid-based RNAiFect system was significantly influenced by the serum incubation, probably due to the nonspecific association with serum proteins. Thus, these results highlighted the excellent feasibility of the PEG-DPT/siRNA complex, particularly under physiological conditions due to the segregation of siRNA into the PEG microenvironment.

The results of the endogenous gene knockdown were more fascinating. For this purpose, a cytoskeletal protein, Lamin A/C, was targeted.[1] The PEG-DPT system showed a significant gene knockdown of Lamin A/C mRNA, even after a 30-min preincubation in 50% serum, evaluated by the real-time RT-PCR analysis. Notably, in 293T cells, the expression was suppressed to the level of 20% of mock samples, which significantly exceeded the ability

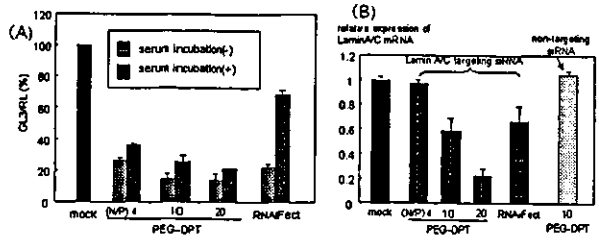

Figure 3. (A) GL3 knockdown by siRNA complexes after serum co-incubation with serum. (B) Endogenous gene (Lamin A/C) knockdown after co-incubation ($n = 4$; ±SD).

of the RNAiFect (Figure 3B). A similar trend was also observed in HuH-7 cells. However, neither the PEG-PLL nor PEG-DMAPA system showed any gene knockdown (data not shown). As Lamin A/C is assumed to abundantly express inside the cells, the threshold level of the siRNA's introduction that is necessary to show the inhibition of gene expression should be significantly higher than in the case of the luciferase cotransfection study. Thus, these results of PEG-DPT were very encouraging for the actual therapeutic knockdown of an endogenous gene by the siRNA delivering approach.

In conclusion, we reported here an effective siRNA nanocarrier system based on the self-assembly of the PEG-based block catiomer. The distinctive polymer design managed both a sufficient siRNA complexation and a buffering capacity of the endosomes. Notably, the siRNA/block catiomer complex revealed remarkable knockdown of the endogenous gene, even after the serum incubation. These results directed this newly designed system of block catiomer to have a promising feasibility for in vivo therapeutics.

Acknowledgment. This work was financially supported by the Core Research Program for Evolutional Science and Technology (CREST) from the Japan Science and Technology Corporation (JST) as well as by Special Coordination Funds for Promoting Science and Technology from the Ministry of Education, Culture, Sports, Science and Technology of Japan (MEXT).

Supporting Information Available: Detailed Materials and Methods section; ^{1}H NMR spectrum of PEG-DPT block copolymer (Figure S1); results of PAGE and EtBr exclusion assay of PEG-DPT (Figure S2); chemical structures of PEG-DMAPA and PEG-PLL (Figure S3); summary of EtBr exclusion assay of these copolymers (Figure S4); and result of MTT assay (Figure S5). This material is available free of charge via the Internet at http://pubs.acs.org.

References

(1) Elbashir, S. M.; Harborth, J.; Lendeckel, W.; Yalcin, A.; Weber, K.; Tuschl, T. *Nature* **2001**, *411*, 494–498.
(2) (a) Kataoka, K.; Togawa, H.; Harada, A.; Yasugi, K.; Matsumoto, T.; Katayose, S. *Macromolecules* **1996**, *29*, 8556–8557. (b) Katayose, S.; Kataoka, K. *Bioconjugate Chem.* **1997**, *8*, 702–707. (c) Vinogradov, S. V.; Bronich, T. K.; Kabanov, A. V. *Bioconjugate Chem.* **1998**, *9*, 805–812. (d) Choi, Y. H.; Liu, F.; Kim, J. S.; Choi, Y. K.; Park, J. S.; Kim, S. W. *J. Controlled Release* **1998**, *54*, 39–48. (e) Ogris, M.; Brunner, S.; Schuller, S.; Kircheis, R.; Wagner, E. *Gene Ther.* **1999**, *6*, 595–605. (f) Oupicky, D.; Konak, C.; Ulbrich, K.; Wolfert, M. A.; Seymour, L. W. *J. Controlled Release* **2000**, *65*, 149–171.
(3) Harada-Shiba, M.; Yamauchi, K.; Harada, A.; Takamisawa, I.; Shimokado, K.; Kataoka, K. *Gene Ther.* **2002**, *9*, 407–414.
(4) Itaka, K.; Yamauchi, K.; Harada, A.; Nakamura, K.; Kawaguchi, H.; Kataoka, K. *Biomaterials* **2003**, *24*, 4495–4506.
(5) Carlson, C.; Beal, P. A. *Biopolymers* **2003**, *70*, 86–102.
(6) Boussif, O.; Lezoualc'h, F.; Zanta, M. A.; Mergny, M. D.; Scherman, D.; Demeneix, B.; Behr, J. P. *Proc. Natl. Acad. Sci. U.S.A.* **1995**, *92*, 7297–7301.

JA047174R

Surface grafting of artificial joints with a biocompatible polymer for preventing periprosthetic osteolysis

TORU MORO[1], YOSHIO TAKATORI[1], KAZUHIKO ISHIHARA[2], TOMOHIRO KONNO[2], YORINOBU TAKIGAWA[3], TOMIHARU MATSUSHITA[4], UNG-IL CHUNG[1], KOZO NAKAMURA[1] AND HIROSHI KAWAGUCHI[1]*

[1]Department of Sensory & Motor System Medicine, Faculty of Medicine, [2]Department of Materials Engineering, School of Engineering, The University of Tokyo, Hongo 7-3-1, Bunkyo, Tokyo 113-0033, Japan
[3]Materials Research and Development Laboratory, Japan Fine Ceramics Center, Atsuta, Nagoya 456-8587, Japan
[4]Japan Medical Materials Corporation, Yodogawa, Osaka 532-0003 Japan
*e-mail: kawaguchi-ort@h.u-tokyo.ac.jp

Published online: 24 October 2004; doi:10.1038/nmat1233

Periprosthetic osteolysis—bone loss in the vicinity of a prosthesis—is the most serious problem limiting the longevity of artificial joints. It is caused by bone-resorptive responses to wear particles originating from the articulating surface. This study investigated the effects of graft polymerization of our original biocompatible phospholipid polymer 2-methacryloyloxyethyl phosphorylcholine (MPC) onto the polyethylene surface. Mechanical studies using a hip-joint simulator revealed that the MPC grafting markedly decreased the friction and the amount of wear. Osteoclastic bone resorption induced by subperiosteal injection of particles onto mouse calvariae was abolished by the MPC grafting on particles. MPC-grafted particles were shown to be biologically inert by culture systems with respect to phagocytosis and resorptive cytokine secretion by macrophages, subsequent expression of receptor activator of NF-κB ligand in osteoblasts, and osteoclastogenesis from bone marrow cells. From the mechanical and biological advantages, we believe that our approach will make a major improvement in artificial joints by preventing periprosthetic osteolysis.

Total joint replacement is the most significant advance in the treatment of osteoarthritis, rheumatoid arthritis and other arthritic diseases affecting major joints of the upper and lower extremities[1]. Despite improvements in implant design and surgical techniques, periprosthetic osteolysis causing aseptic loosening of artificial joints remains the most serious problem limiting their survival and clinical success[2].

Pathogenesis of the periprosthetic osteolysis is known to be a consequence of the host inflammatory response to wear particles originating from the prosthetic devices[1,2]. Many clinical and animal studies have shown that the most abundant and bone-resorptive particle within the periprosthetic tissues is polyethylene (PE) generated from the interface between the PE and metal components[3–5]. A key role has generally been attributed to the phagocytosis of the PE particles by macrophages, followed by secretion of prostaglandin E_2 (PGE_2) and the cytokines tumour necrosis factor-α (TNF-α), interleukin-1 (IL-1) and IL-6 (ref. 6). These bone-resorptive factors induce the expression of a receptor activator of NF-kB ligand, the key member-associated molecule for osteoclastogenesis, in osteoblasts, consequently resulting in osteoclastic bone resorption[2,7,8]. Hence, reducing the production of wear particles and bone-resorptive responses may lead to the elimination of periprosthetic osteolysis. Based on this hypothesis, we prepared a novel hip PE component grafted with MPC onto its surface. The MPC polymer is our original biocompatible polymer whose side chain is composed of phosphorylcholine resembling phospholipids of biomembranes (Fig. 1a)[9]. The MPC grafting onto the surface of medical devices has already been shown to suppress biological reactions even when they are in contact with living organisms[10,11], and is now clinically used on the surfaces of intravascular stents, intravascular guide wires, soft contact lenses and the oxygenator (artificial lung) under the authorization of the Food and Drug Administration of the United States[12–14]. The present study investigated the mechanical and biological effects of the MPC grafting onto the surface of the PE component of artificial joints.

Grafting of the MPC onto the PE surface of hip acetabular liners was performed by a photoinduced polymerization technique, producing a covalent bond between the MPC and PE polymers (Fig. 1a)[15]. The stable grafting of MPC on the PE was confirmed using highly sensitive X-ray photoelectron spectroscopy (XPS; PHI5400MC, Perkin Elmer, USA) (Fig. 1b). The peaks in the carbon atom region (C_{1s}) at 286.5eV and 289 eV, indicating the ether

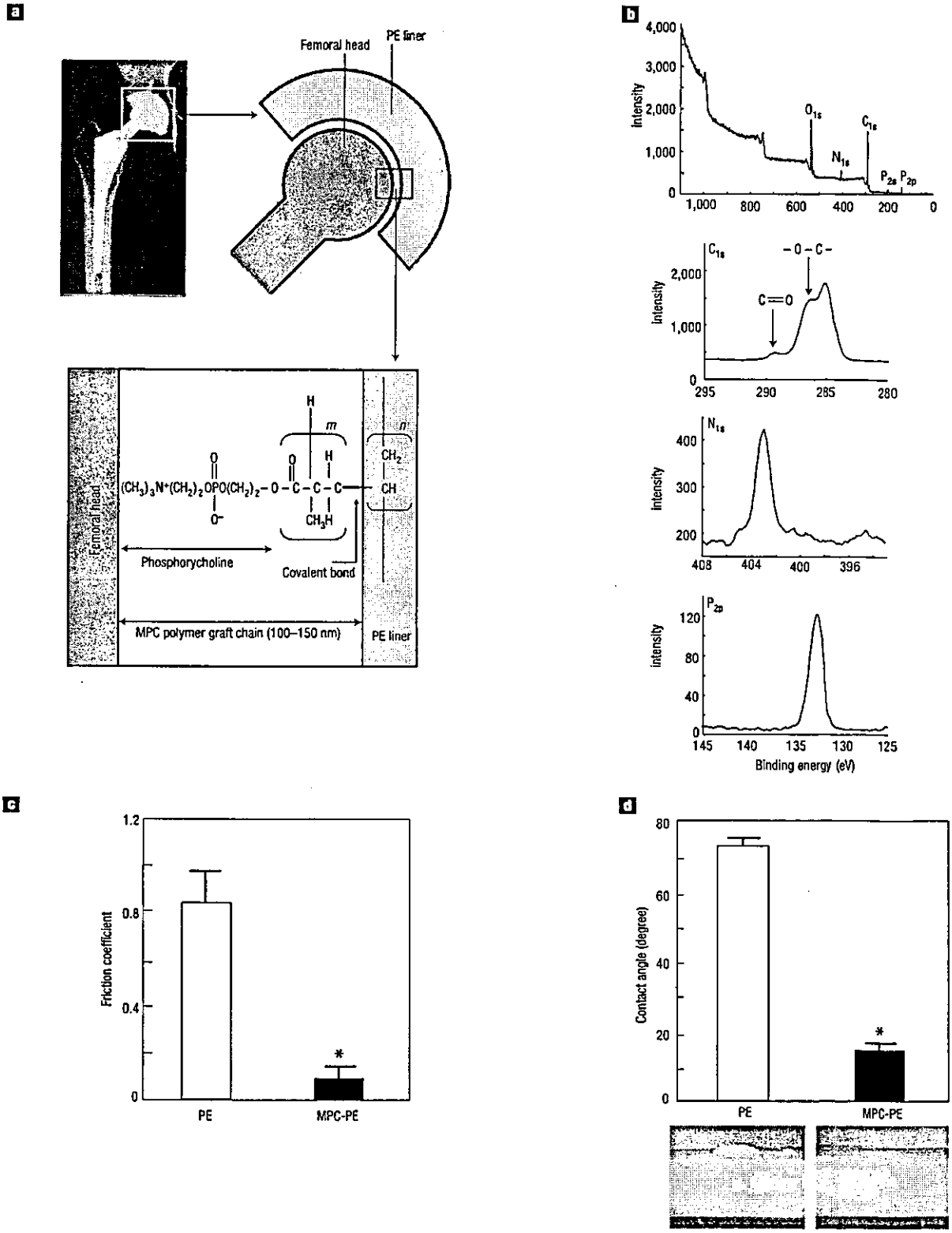

Figure 1 Surface analyses of the MPC grafted PE. a, Upper left shows an X-ray of a replaced hip joint in which the relationship between the femoral head and the PE liner is indicated at upper right. MPC is bound to the PE liner by the covalent bond with a photoinduced graft polymerization technique. **b**, XPS charts of the PE liner surface with the MPC grafting. The peaks in the carbon (C_{1s}), nitrogen (N_{1s}) and phosphorus (P_{2p}) atom regions are specific to the MPC, indicating successful grafting. **c**, Lubricity determined by the friction coefficient of PE plates with and without the MPC grafting (MPC-PE and PE, respectively). **d**, Hydrophilicity determined by the contact angle of a water drop with PE and MPC-PE plates. Representative pictures are shown below. Data are expressed as means (bars) ± s.e.m. (error bars) for 12 plates per group. * significant difference from PE; $P<0.01$.

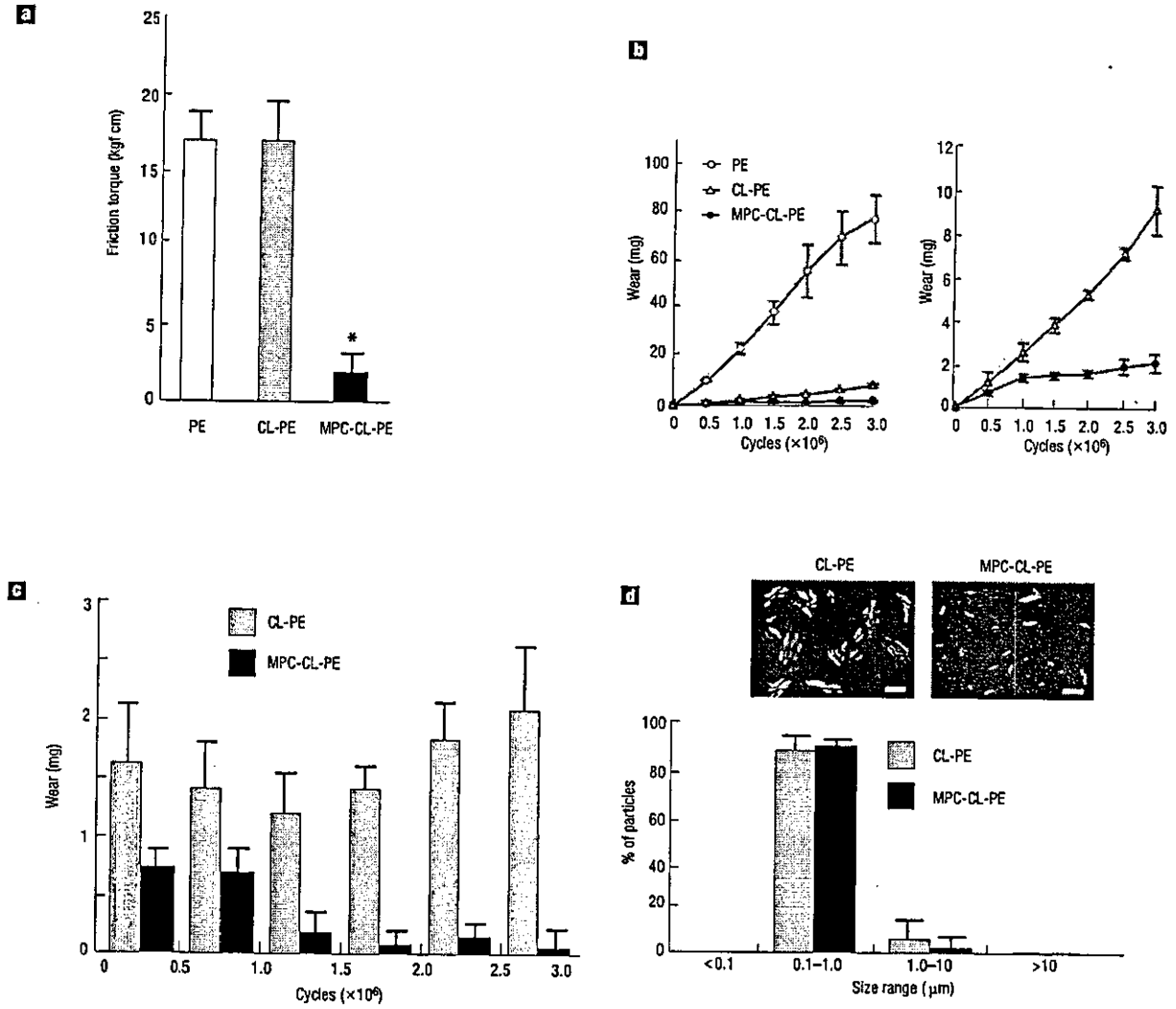

Figure 2 The friction torque and the wear amount in the hip-joint simulator with three kinds of PE liners. a, Friction torque of the three liners against the femoral heads measured before the loading test. b, Time course of the wear amount produced from the three liners during 3×10^6 cycles of loading. The CL-PE and MPC-CL-PE data are shown in an expanded scale on the right. c, The wear amount from the CL-PE and MPC-CL-PE liners for every 5×10^5 cycle intervals. d, Representative SEM images of the wear particles isolated from lubricants of the simulators with CL-PE and MPC-CL-PE liners. The graph below shows the distribution of particles in each size range. Data are expressed as means (symbols and bars) ± s.e.m. (error bars) for 10 liners per group. * significant difference from PE; $P<0.01$.

bond and the ester bond, respectively, and those in the nitrogen atom at 403 eV (N_{1s}) and phosphorus atom at 133 eV (P_{2p}) were specific to the phosphorylcholine group in the MPC unit.

To assess the lubricity and hydrophilicity, the MPC was grafted onto the PE plate (MPC-PE plate). The friction coefficient measured using a tensile test device and the contact angle of a water drop measured using the sessile drop method with a goniometer on the MPC-PE plate were about 1/7 and 1/5, respectively, of those on the non-grafted PE plate (Fig. 1c,d). These results indicate that the MPC grafting on PE greatly increases both lubricity and hydrophilicity.

Mechanical effects of the MPC grafting on the hip prosthesis were examined using a hip-joint wear simulator[16] under the conditions recommended by the International Organization for Standardization (ISO). We prepared crosslinked acetabular PE liners with photoinduced grafting of MPC onto their surface (MPC-CL-PE liner), and compared them with crosslinked PE liners without the MPC grafting (CL-PE liner) and non-crosslinked PE liners without the MPC grafting (PE liner). The friction torques of the three liners against the femoral head were compared before the loading test. There was no difference between PE and CL-PE liners; however, the MPC-CL-PE liner showed 80–90% lower torque than these two (Fig. 2a). Throughout the 3×10^6 cycles of gravimetric loading by the hip-joint simulator, the wear amount of the MPC-CL-PE liner was about 4 and 40 times less than those of the CL-PE and the PE liners, respectively (Fig. 2b). Clinically, the wear rate at the initial stage after a total hip replacement is thought to be well correlated with the incidence of periprosthetic osteolysis, because the wear particles may gain access to the articulation and accelerate the additional wear by a three-body mechanism[17]. In fact, the time-course analysis of the wear amount for every 5×10^5 cycle intervals

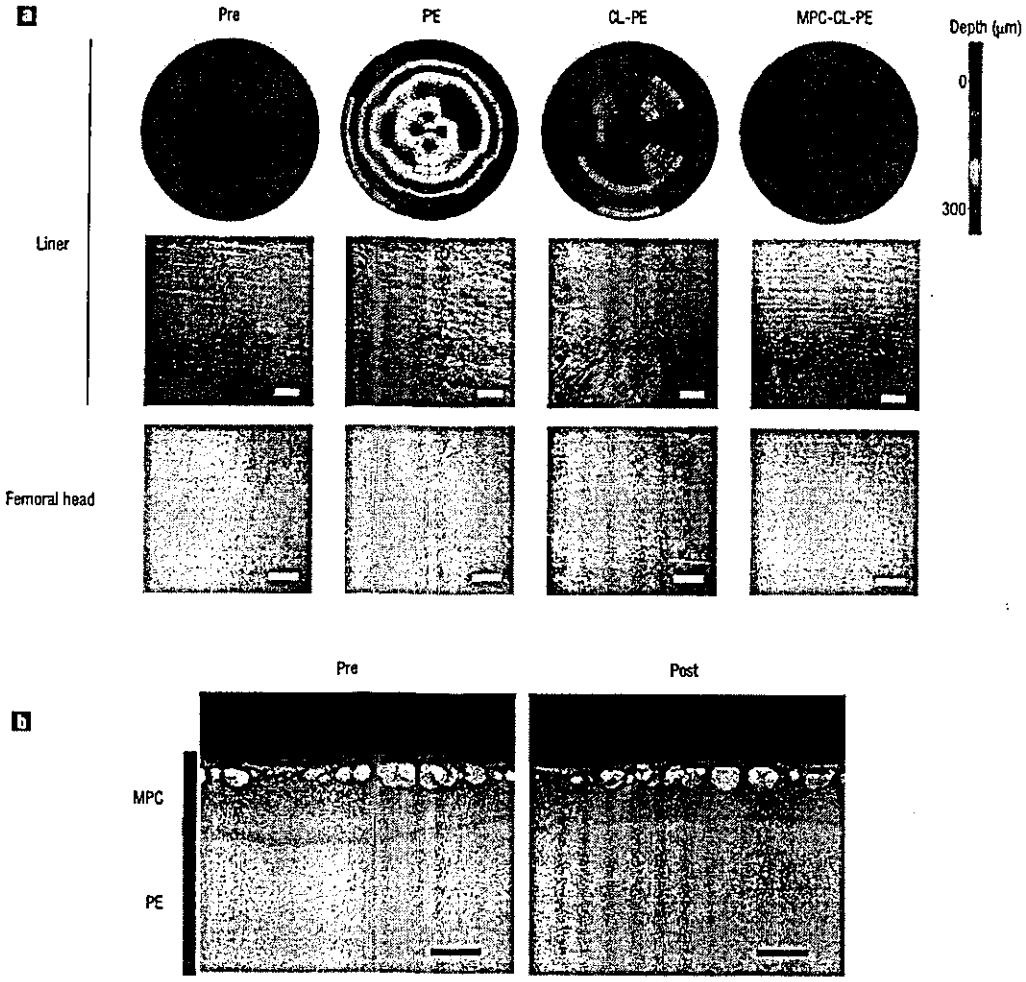

Figure 3 Optical findings of the surfaces of liners and corresponding femoral heads. a, Three-dimensional morphometric and SEM analyses of the liner surfaces (top and middle, respectively) and SEM analyses of the femoral head surfaces (bottom) before (Pre) and after 3×10^6 cycles of loading. Scale bars, 500 μm and 20 μm in middle and bottom, respectively. **b**, FE-TEM images of the thickness of MPC layer before (Pre) and after (Post) the loading. The bubbles on the surface were produced in the process of preparing the specimen. Scale bars, 100 nm.

revealed that the amount from the CL-PE liner was about twice as large as that from the MPC-CL-PE in the initial cycles, and somewhat increased in the later cycles (Fig. 2c). Contrarily, about 70% of the total wear amount was produced from the MPC-CL-PE liner in the initial 1×10^6 cycles, and decreased thereafter. In the last 5×10^5 cycles, the wear amount of MPC-CL-PE was less than 1/20 that of CL-PE. Although the present 3×10^6 cycles of 280 kgf (kilogram force) load is assumed equivalent to 3–10 years of physical walking, this result suggests that the mechanical effect of the MPC grafting will be maintained or somewhat more pronounced even after loading beyond 3×10^6 cycles. In fact, our preliminary simulator experiment with 1×10^7 cycles of loading revealed much stronger wear resistance by this grafting (data not shown). Scanning electron microscopy (SEM; JSM-5800LV, JEOL, Tokyo, Japan) analysis of the wear particles isolated from the lubricants revealed no significant difference of the particle size distribution between CL-PE and MPC-CL-PE liners, the great majority of which was 0.1–1.0 μm (Fig. 2d).

Optical examination of the liner surface using a three-dimensional morphometric analysis after 3×10^6 cycles of loading revealed that there was little or no wear in the MPC-CL-PE liner, whereas substantial wear was detected in the PE and CL-PE liners (Fig. 3a, top). The SEM analysis of the liner surface revealed that the original machine marks by the manufacturer's processing still remained on the MPC-CL-PE liner surface, which were completely obliterated in the two control liners (Fig. 3a, middle). Furthermore, the field emission transmission electron microscopy (FE-TEM) analysis showed that most of the liner surface was covered by the MPC polymer layer even after 3×10^6 cycles of loading (Fig. 3b). The XPS analysis also confirmed the remainder of the specific spectra of C_{1s}, P_{2p} and N_{1s} on the MPC-PE liner surface just as in Fig. 1b after the loading (data not shown). Contrarily, the SEM analysis of the femoral head showed no difference among the three groups (Fig. 3a, bottom). The femoral heads were free of visible scratches and the surface roughness expressed by the R_a values was not different before or after the loading in all groups (R_a = 0.05–0.06 μm), suggesting there was no abrasive contamination with metal particles from the heads in the hip-joint simulator.

With respect to the reduction of wear by the MPC grafting, we should consider the lubrication mechanism between the liners and

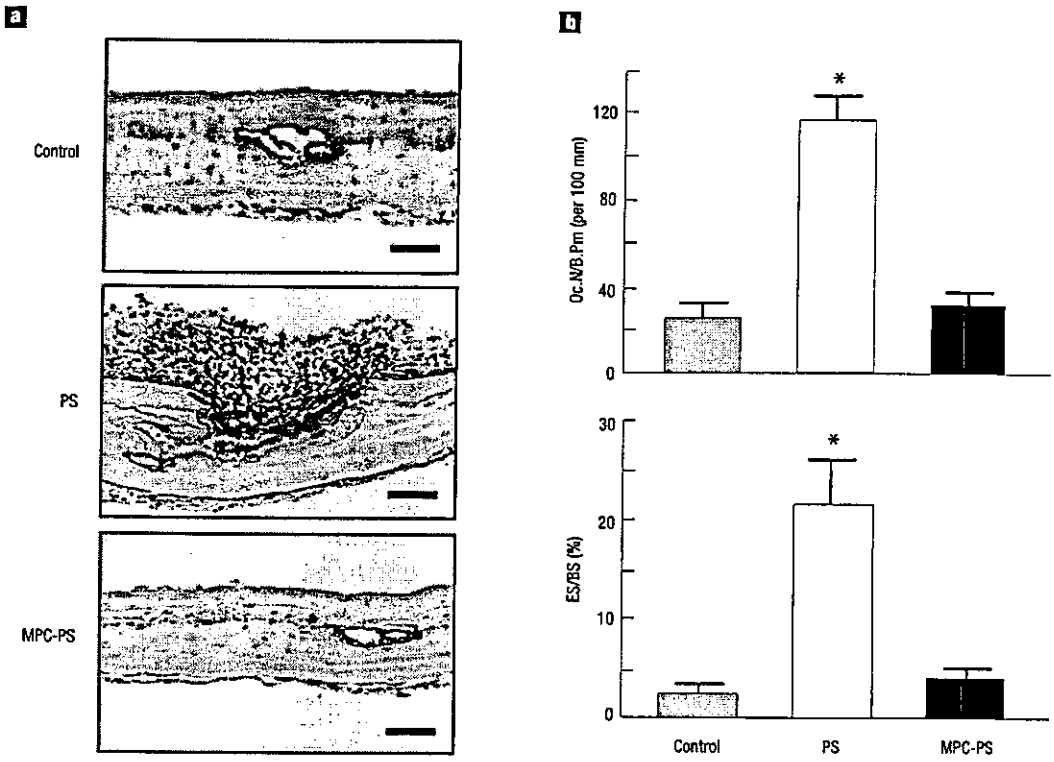

Figure 4 ***In vivo*** **bone resorption in mouse calvariae.** Resorption induced by a subperiosteal injection of an aliquot of PS particles with and without the MPC grafting (MPC-PS and PS, respectively) or an equal volume of solvent alone (control). **a**, Representative histological findings of the injected sites where osteoclasts were stained red with TRAP. Scale bars, 100 μm. **b**, Histomorphometric analyses of the injected sites: number of mature osteoclasts in 100 mm of bone perimeter (Oc.N/B.Pm; top) and percentage of eroded surfaces (ES) / bone surfaces (BS) (bottom). Data are expressed as means (bars) ± s.e.m. (error bars) for 8 calvariae per group. * significant difference from control; $P<0.01$.

metal heads of the hip-joint simulator. Although phospholipids themselves are known to work as effective boundary lubricants[18,19], recent studies of natural synovial joints have shown that fluid film lubrication by the intermediate hydrated layer is the predominant mechanism under physiological walking conditions[20]. Because the present study revealed that the MPC grafting onto the PE plate increased the hydrophilicity (Fig. 1d) and our previous study showed that the free-water fraction on the MPC polymer surface is kept at a higher level[21], the reduction of wear is likely to arise from the hydrated lubricating layer that is formed by the MPC grafting.

As PE particles are known to be most abundant and catabolic among wear particles in the periprosthetic tissues[3–5], alternative bearing surfaces have been proposed such as ceramic-on-ceramic and metal-on-metal articulations; however, these have their own potential disadvantages[22,23]. The long history and popularity of PE as a bearing surface has led to research in the development of tougher and more wear-resistant PE materials: the incorporation of short chopped carbon fibres in PE matrix (Poly II)[3,24], the extension of chain crystallite morphology with thicker lamellae and higher crystallinity (Hylamer)[25], and the creation of a three-dimensional molecular network by the crosslinking. Among them, only the crosslinking successfully improved the wear resistance and suppressed the periprosthetic osteolysis in the clinical setting[26,27]. It is therefore noteworthy that the MPC grafting onto the crosslinked PE surface further increased the wear resistance over the conventional crosslinked PE.

Considering that MPC is a biocompatible polymer, we next examined biological responses to particles using *in vivo* and *in vitro* models. The MPC polymer was grafted using a solvent-evaporation technique onto the surface of polystyrene (PS) particles whose size was approximately 500 nm in diameter, based on the result above (Fig. 2d) and previous findings[5,28] that the mean particle size from clinically failed prostheses is around 500 nm with >90% of particles less than 1 μm. The XPS spectra of C_{1s}, P_{2p} and N_{1s} on the surface of the PS particles grafted with MPC were quite similar to that of the MPC-PE liner surface as shown in Fig. 1b (data not shown). Although the surface electrical potential (ζ-potential) of the surface of non-grafted PS particles determined using electrophoretic light scattering was around −66.0 mV, the MPC grafting neutralized the potential to −2.5 mV, as we reported previously[29]. These results indicate that the MPC polymer was stably immobilized on the surface of the particles.

We first compared the *in vivo* bone resorption induced by PS particles with and without the MPC grafting using an established *in vivo* murine calvarial model[7,30]. When non-treated PS particles were injected beneath the calvarial periosteum, notable stimulations of tartrate-resistant acid phosphatase (TRAP)-positive osteoclast formation and bone resorption with inflammatory reaction were observed (Fig. 4a). However, subperiosteal injection of the MPC-grafted particles did not induce bone resorption. This effect was confirmed by histomorphometric analysis: the osteoclast number and the eroded surface of the calvarial bone that were increased

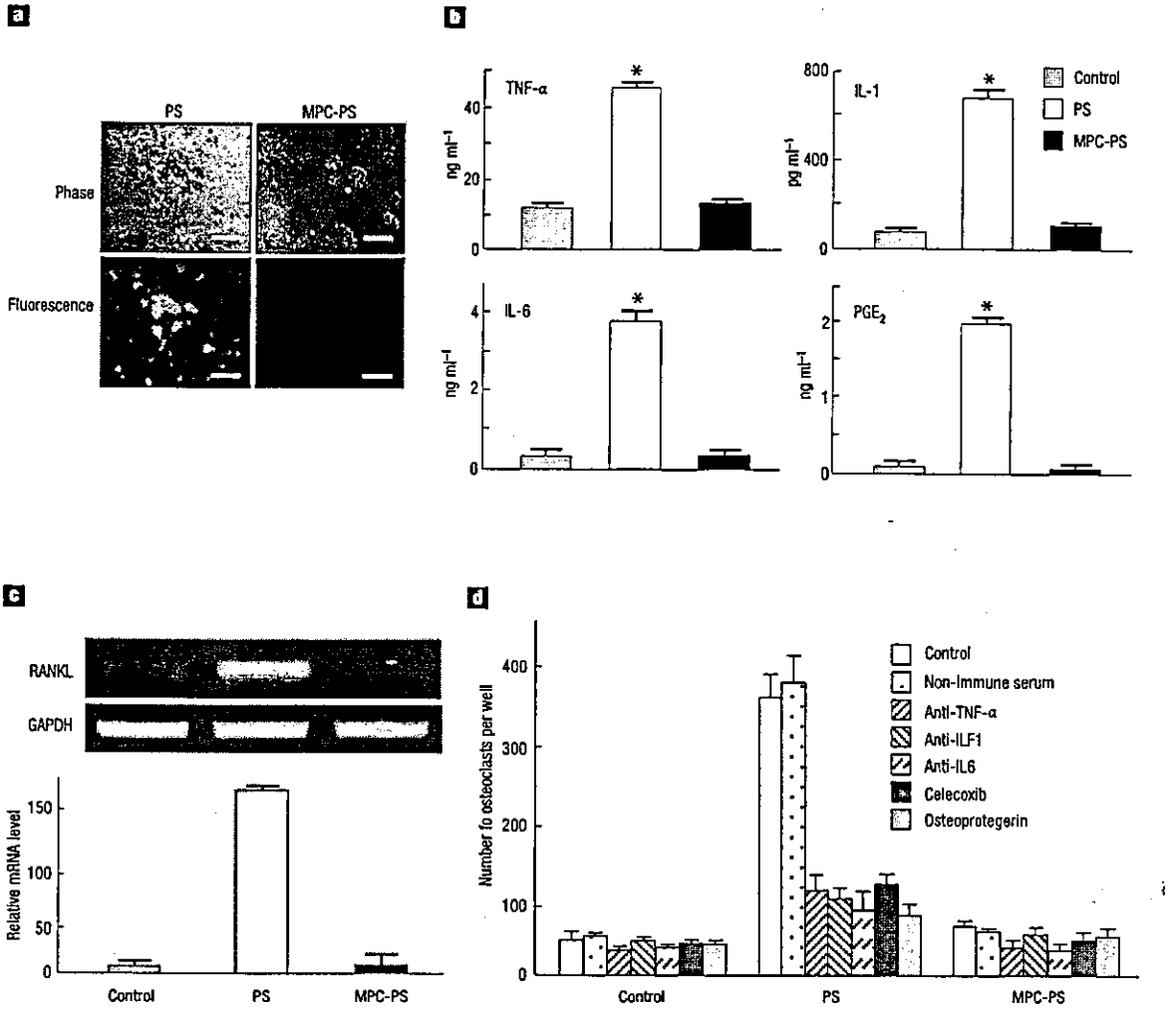

Figure 5 Bone-resorptive responses in cultures exposed to PS particles with and without the MPC grafting (MPC-PS and PS, respectively). **a**, Phagocytosis of fluorescence-labelled particles by cultured mouse intraperitoneal macrophages. Phase: phase contrast microscopic image. Fluorescence: fluorescence microscopic image. Scale bars, 100 μm. **b**, Concentrations of bone-resorptive factors TNF-α, IL-1, IL-6 and PGE_2 in the supernatants of the mouse macrophage-like cell line J774 culture with or without exposure to particles. **c**, RANKL expression by mouse primary osteoblasts isolated from neonatal mouse calvariae and cultured in the three kinds of conditioned media of the J774 cell cultures above. RANKL mRNA levels were determined by semiquantitative RT-PCR (top) and real-time RT-PCR (bottom). GAPDH is glyceraldehyde 3-phosphate dehydrogenase. **d**, Osteoclastogenesis in the coculture of mouse bone marrow cells and osteoblasts by the three kinds of conditioned media of J774 cells above, and inhibition by antagonists to cytokines, PGs and RANKL. Osteoclastogenesis was determined by the number of TRAP-positive multinucleated cells. Data are expressed as means (bars) ± s.e.m. (error bars) for 8–12 cultures per group. * significant difference from control; $P<0.01$.

four- to sixfold by the implantation of non-treated PS particles, as compared with those by the solvent alone, but were little affected by the MPC-grafted particles, indicating that MPC grafting is biologically inert (Fig. 4b).

To further investigate the cellular and molecular mechanisms underlying the prevention of osteoclastic bone resorption by the MPC grafting, we first compared the phagocytosis of fluorescence-labelled PS particles with and without the MPC grafting by cultured mouse intraperitoneal macrophages. Although large amounts of non-treated particles were phagocytosed by macrophages, the MPC-grafted particles were not taken into the cells, probably because biocompatible MPC polymer prevented macrophages from recognizing the particles as foreign bodies (Fig. 5a). We next examined the secretion of bone-resorptive factors by macrophages exposed to the particles. Concentrations of TNF-α, IL-1, IL-6 and PGE_2 in the culture medium of mouse macrophage-like cell line J774 cells were 4–20 times more stimulated by the exposure to non-treated PS particles than those without the exposure; however, the exposure to the MPC-grafted particles affected none of them (Fig. 5b). When the conditioned media of J774 cells were added to a mouse osteoblast culture, the receptor of NF-kB ligand (RANKL) was strongly expressed by the medium exposed to non-treated particles, but not by that exposed to the MPC-grafted particles (Fig. 5c). These results indicate that the MPC grafting prevented the secretion of resorptive factors by macrophages and the subsequent RANKL expression by osteoblasts. Finally, osteoclastogenesis in the coculture of mouse bone marrow cells and osteoblasts was increased about sevenfold by the conditioned medium of J774 cells exposed

to non-treated PS particles as compared with the control, and this stimulation was significantly inhibited by addition of anti-TNF-α, anti-IL-1 or anti-IL-6 antibody, a cyclooxygenase-2 (COX-2) inhibitor celecoxib, and a RANKL inhibitor osteoprotegerin; this confirmed the involvement of some network systems of these factors in the osteoclastogenesis by wear particles. Contrarily, the conditioned medium of J774 cells exposed to the MPC-grafted particles did not increase osteoclastogenesis (Fig. 5d). These biological findings indicate that the MPC grafting can successfully inhibit the bone-resorptive response to wear particles to levels similar to those of recently developed pharmacological therapies such as cytokine antagonists, COX-2 inhibitors and osteoprotegerin[7,8]. Because the lack of side effects of the MPC grafting has already been confirmed clinically by several medical devices[12–14], this surface grafting will surpass the pharmacologic therapies that possibly cause serious side effects during a long period of administration after surgery.

For these biological studies, we initially tried to use the PE wear particles isolated from the hip-simulator experiment above; however, it turned out to be impossible because the PE particles could not be isolated from the lubricants without damaging the MPC polymer layer. The lubricants after loading contain abundant and adhesive proteins that were degraded and precipitated by the heat generated by the head-liner friction. For the isolation of PE particles, it is essential to digest the proteins using strong hydroxide[28,31,32], which cannot avoid breaking the chemical structure such as the esteratic bond of the MPC unit. In fact, the XPS analysis of the surface of isolated particles revealed the lack of the MPC polymer layer. In addition, even if we could isolate the PE particles with MPC grafting properly, the amount from the MPC-CL-PE liner was too small to be used for the biological experiments. We therefore attempted to graft MPC onto the surface of new PE particles or the wear particles from the simulator experiment; however, the floating nature of PE on the liquid surface due to the low specific gravity made the photoinduced polymerization of MPC impossible, because the grafting procedure requires that the particles be agitated in the liquid[29]. Hence, for the biological experiments we used PS particles that have conventionally been used for the *in vivo* and *in vitro* analyses of particle-induced osteolysis as a substitute for PE[6,33,34]. PS is a hydrocarbon polymer just like PE, but has a higher specific gravity than PE. Because these two polymers share similar physical and chemical properties—electrically neutral and little chemical sensitivity—we believe that biological responses to these particles are also similar.

Taken together, the present results demonstrate that grafting MPC onto the PE liner surface of the hip prosthesis markedly decreased the friction and the production of wear particles. In addition, even if the particles were produced by friction, they were biologically inert with respect to phagocytosis by macrophages and subsequent bone-resorptive responses: secretion of cytokines and PGE_2, induction of RANKL, and osteoclastogenesis.

Although this study focused on the hip prosthesis, whose loosening is the most frequent and serious among total joint replacements of upper and lower extremities, the MPC grafting can be used for the prevention of periprosthetic osteolysis of other joints, in which PE particles from articular interfaces are also known to initiate the catabolic cascade[35,36]. From the mechanical and biological advantages shown in this study, we believe that the MPC grafting will make a significant improvement in total joint replacements by preventing periprosthetic osteolysis and aseptic loosening. The development of this technique would improve the quality of care of patients having total joint replacements and have a substantial public health impact. We are now designing a large-scale clinical trial.

METHODS

For mechanical analyses, a 12-station hip-joint wear simulator apparatus (MTS, MTS Systems, Minneapolis, Minnesota) with three kinds of PE liners in 42 mm acetabular cups: non-crosslinked PE liner (K-MAX, Japan Medical Materials, Osaka), crosslinked PE liner (K-MAX Excellink), and MPC-grafted K-MAX Excellink, coupled to 22 mm cobalt–chromium–molybdenum alloy heads (K-MAX HH-02, Excellink), was mounted on rotating blocks to produce biaxial or orbital motion[16]. The simulator experiment was performed according to the international standard of "implants for surgery – wear of total hip-joint prosthesis" established by ISO (#14242-1; 2002), which was proved to be closest to the physiological conditions. Briefly, a Paul-type loading profile, which is a physiological walking simulation with continuous cyclic motion and loading, was applied (maximum force = 280 kgf, frequency = 1 Hz)[17] in the lubricant of distilled water containing 25% bovine calf serum. Friction torque between the liner and the femoral head was measured using a torque measuring instrument. The simulator was run up to 3×10^6 cycles, and the change of lubricant and gravimetric measurement of the liners were performed every 5×10^5 cycles. For the isolation of wear particles, the lubricant after the loading was incubated with 5 N NaOH solution in order to digest adhesive proteins that were degraded and precipitated; the particles were then collected and underwent sequential filtrations, as reported previously[32]. The size of particles was defined as the maximum dimensions by SEM analysis.

For biological analyses, all animal experiments were performed according to the guidelines of the International Association for the Study of Pain[38], and were approved by the committee of Tokyo University charged with confirming ethics. The *in vivo* mouse calvaria experiment was performed as reported previously[7,39]. Briefly, after exposing the calvaria of mice, a subperiosteal injection of PS particles (average diameter = 468 nm; Polysciences, Warrington, Pennsylvania) with or without the MPC grafting, or an equal volume of solvent (deionized water) alone was performed.

Mice were sacrificed seven days after the surgery, and the calvaria was excised, fixed, and decalcified in EDTA. Osteoclastogenesis in the coronal histological sections was determined by TRAP staining. The sections were subjected to histomorphometric analyses under a light microscope with a micrometer, and parameters for bone resorption were measured as reported previously[39]. For the phagocytosis experiment, mouse intraperitoneal macrophages were isolated, exposed to fluorescence-labelled particles, cultured for 1 h, and observed with a fluorescence microscope. Mouse macrophage-like cell line J774 cells (Riken Cell Bank, Saitama, Japan) were exposed to particles and cultured for 24 h. The supernatants were subject to cytokine and PGE_2 measurements using the ELISA method, and were used as the conditioned media for the following assays. For the RANKL expression assay, mouse osteoblasts isolated from neonatal calvariae were cultured in the conditioned media for 24 h. RANKL expression in osteoblasts was measured using the semi-quantitative and real-time reverse transcription polymerase chain reaction (RT-PCR) analyses. The information on the primers is available upon request. For osteoclast formation assay, mouse primary osteoblasts above and bone marrow cells isolated from adult mouse long bones were cocultured in the conditioned media in the presence or absence of anti-TNF-α, anti-IL1, anti-IL-6 antibody, control non-immune serum, celecoxib or osteoprotegerin. Cells were stained with TRAP, and those positively stained and containing more than three nuclei were counted as osteoclasts. For the statistical analysis, means of groups were compared by ANOVA and the significance of differences was determined by post-hoc testing using Bonferroni's method.

Received 13 April 2004; accepted 9 Augsut 2004; published 24 October 2004.

References

1. Harris, W. H. Wear and periprosthetic osteolysis: the problem. *Clin. Orthop.* 393, 66–70 (2001).
2. Jacobs, J. J., Roebuck, K. A., Archibeck, M., Hallab, N. J. & Glant, T. T. Osteolysis: basic science. *Clin. Orthop.* 393, 71–77 (2001).
3. Connelly, G. M., Rimnac, C. M., Wright, T. M., Hertzberg, R. W. & Manson, J. A. Fatigue crack propagation behavior of ultrahigh molecular weight polyethylene. *J. Orthop. Res.* 2, 119–125 (1984).
4. von Knoch, M. *et al.* The effectiveness of polyethylene versus titanium particles in inducing osteolysis in vivo. *J. Orthop. Res.* 22, 237–243 (2004).
5. Maloney, W. J. *et al.* Isolation and characterization of wear particles generated in patients who have had failure of a hip arthroplasty without cement. *J. Bone Joint Surg. Am.* 77, 1301–1310 (1995).
6. Glant, T. T. *et al.* Bone resorption activity of particulate-stimulated macrophages. *J. Bone Miner. Res.* 8, 1071–1079 (1993).
7. Childs, L. M. *et al.* In vivo RANK signaling blockade using the receptor activator of NF-κB:Fc effectively prevents and ameliorates wear debris-induced osteolysis via osteoclast depletion without inhibiting osteogenesis. *J. Bone Miner. Res.* 17, 192–199 (2002).
8. Goater, J. J., O'Keefe, R. J., Rosier, R. N., Puzas, J. E. & Schwarz, E. M. Efficacy of ex vivo OPG gene therapy in preventing wear debris induced osteolysis. *J. Orthop. Res.* 20, 169–173 (2002).
9. Ishihara, K., Ueda, T. & Nakabayashi, N. Preparation of phospholipid polymers and their properties as polymer hydrogel membrane. *Polym. J.* 22, 355–360 (1990).
10. Ishihara, K., Shinozuka, T., Hanazaki, Y., Iwasaki, Y. & Nakabayashi, N. Improvement of blood compatibility on cellulose hemodialysis membrane: IV. Phospholipid polymer bonded to the membrane surface. *J. Biomater. Sci. Polym. Edn* 10, 271–282 (1999).
11. Yoneyama, T., Sugihara, K., Ishihara, K., Iwasaki, Y. & Nakabayashi, N. The vascular prosthesis without pseudointima prepared by antithrombogenic phospholipid polymer. *Biomaterials* 23, 1455–1459 (2002).
12. Kihara, S. *et al.* In vivo evaluation of a MPC polymer coated continuous flow left ventricular assist system. *Artif. Organs* 27, 188–192 (2003).
13. Lewis, A. L. Phosphorylcholine-based polymers and their use in the prevention of biofouling. *Colloids Surf. B* 18, 261–275 (2000).
14. Lewis, A. L., Tolhurst, L. A. & Stratford, P. W. Analysis of a phosphorylcholine-based polymer coating on a coronary stent pre- and post-implantation. *Biomaterials* 23, 1697–1706 (2002).
15. Ishihara, K., Iwasaki, Y., Ebihara, S., Shindo, Y. & Nakabayashi, N. Photoinduced graft polymerization of 2-methacryloyloxyethyl phosphorylcholine on polyethylene membrane surface for obtaining blood cell adhesion resistance. *Colloids Surf. B* 18, 325–335 (2000).
16. Nakamura, T. *et al.* Clinical and laboratory wear studies of zirconia-on-UHMWPE combination in cementless THA. *Key Eng. Mater.* 240–242, 823–826 (2003).
17. Sochart, D. H. Relationship of acetabular wear to osteolysis and loosening in total hip arthroplasty. *Clin. Orthop.* 363, 135–150 (1999).
18. Williams, P. P. 3rd, Powell, G. L. & LaBerge, M. Sliding friction analysis of phosphatidylcholine as a boundary lubricant for articular cartilage. *Proc. Inst. Mech. Eng. H* 207, 59–66 (1993).

19. Hills, B. A. Boundary lubrication in vivo. *Proc. Inst. Mech. Eng. H* **214**, 83–94 (2000).
20. Dowson, D. & Jin, Z. M. Micro-elastohydrodynamic lubrication of synovial joints. *Eng. Med.* **15**, 63–65 (1986).
21. Ishihara, K. *et al.* Why do phospholipid polymers reduce protein adsorption? *J. Biomed. Mater. Res.* **39**, 323–330 (1998).
22. Black, J. Metal on metal bearings. A practical alternative to metal on polyethylene total joints? *Clin. Orthop.* **329**, S244–S255 (1996).
23. Callaway, G. H., Flynn, W., Ranawat, C. S. & Sculco, T. P. Fracture of the femoral head after ceramic-on-polyethylene total hip arthroplasty. *J. Arthroplasty* **10**, 855–859 (1995).
24. Wright, T. M., Rimnac, C. M., Faris, P. M. & Bansal, M. Analysis of surface damage in retrieved carbon fiber-reinforced and plain polyethylene tibial components from posterior stabilized total knee replacements. *J. Bone Joint Surg. Am.* **70**, 1312–1319 (1988).
25. Livingston, B. J., Chmell, M. J., Spector, M. & Poss, R. Complications of total hip arthroplasty associated with the use of an acetabular component with a Hylamer liner. *J. Bone Joint Surg. Am.* **79**, 1529–1538 (1997).
26. Kurtz, S. M., Muratoglu, O. K., Evans, M. & Edidin, A. A. Advances in the processing, sterilization, and crosslinking of ultra-high molecular weight polyethylene for total joint arthroplasty. *Biomaterials* **20**, 1659–1688 (1999).
27. McKellop, H., Shen, F. W., DiMaio, W. & Lancaster, J. G. Wear of gamma-crosslinked polyethylene acetabular cups against roughened femoral balls. *Clin. Orthop.* **369**, 73–82 (1999).
28. Ingram, J. H., Stone, M., Fisher, J. & Ingham, E. The influence of molecular weight, crosslinking and counterface roughness on TNF-alpha production by macrophages in response to ultra high molecular weight polyethylene particles. *Biomaterials* **25**, 3511–3522 (2004).
29. Konno, T., Kurita, K., Iwasaki, Y., Nakabayashi, N. & Ishihara, K. Preparation of nanoparticles composed with bioinspired 2-methacryloyloxyethyl phosphorylcholine polymer. *Biomaterials* **22**, 1883–1889 (2001).
30. Boyce, B. F., Aufdemorte, T. B., Garrett, I. R., Yates, A. J. & Mundy, G. R. Effects of interleukin-1 on bone turnover in normal mice. *Endocrinology* **125**, 1142–1150 (1989).
31. Campbell, P. *et al.* Isolation of predominantly submicron-sized UHMWPE wear particles from periprosthetic tissues. *J. Biomed. Mater. Res.* **29**, 127–131 (1995).
32. Jono, K., Takigawa, Y., Takadama, H., Mizuno, M. & Nakamura, T. A multi-station hip joint simulator study and wear characterization of commercial hip endoprostheses. *Ceram. Eng. Sci. Proc.* **24**, 255–260 (2003).
33. Vermes, C. *et al.* The effects of particulate wear debris, cytokines, and growth factors on the functions of MG-63 osteoblasts. *J. Bone Joint Surg. Am.* **83**, 201–211 (2001).
34. Yao, J., Cs-Szabo, G., Jacobs, J. J., Kuettner, K. E. & Glant, T. T. Suppression of osteoblast function by titanium particles. *J. Bone Joint Surg. Am.* **79**, 107–112 (1997).
35. Inagaki, K. *et al.* Importance of a radial head component in Sorbie unlinked total elbow arthroplasty. *Clin. Orthop.* **400**, 123–131 (2002).
36. Shanbhag, A. S. *et al.* Quantitative analysis of ultrahigh molecular weight polyethylene (UHMWPE) wear debris associated with total knee replacements. *J. Biomed. Mater. Res.* **53**, 100–110 (2000).
37. Paul, J. P. Forces transmitted by joints in the human body. *Proc. Inst. Mech. Eng.* **181**, 8–15 (1967).
38. Zimmermann, M. Ethical guidelines for investigations of experimental pain in conscious animals. *Pain* **16**, 109–110 (1983).
39. Ogata, N. *et al.* Insulin receptor substrate-1 in osteoblast is indispensable for maintaining bone turnover. *J. Clin. Invest.* **105**, 935–943 (2000).

Acknowledgements

We thank Noboru Yamawaki, Takatoshi Miyashita, Hiroaki Takadama, Kaori Jono, Reiko Yamaguchi, and Mizue Ikeuchi for their excellent technical help. This work was supported by Grants-in-Aid for Scientific Research from the Japanese Ministry of Education, Culture, Sports, Science and Technology (#15390449), and Health and Welfare Research Grant for Comprehensive Research on Aging and Health from the Japanese Ministry of Health, Labour and Welfare.

Correspondence and requests for materials should be addressed to H.K.

Supplementary Information accompanies the paper on www.nature.com/naturematerials

Competing financial interests

The authors declare that they have no competing financial interests.

ARTHRITIS & RHEUMATISM
Vol. 50, No. 11, November 2004, pp 3561–3573
DOI 10.1002/art.20611

The Combination of SOX5, SOX6, and SOX9 (the SOX Trio) Provides Signals Sufficient for Induction of Permanent Cartilage

Toshiyuki Ikeda,[1] Satoru Kamekura,[2] Akihiko Mabuchi,[1] Ikuyo Kou,[1] Shoji Seki,[1] Tsuyoshi Takato,[3] Kozo Nakamura,[2] Hiroshi Kawaguchi,[2] Shiro Ikegawa,[1] and Ung-il Chung[3]

Objective. **To regenerate permanent cartilage, it is crucial to know not only the necessary conditions for chondrogenesis, but also the sufficient conditions. The objective of this study was to determine the signal sufficient for chondrogenesis.**

Methods. **Embryonic stem cells that had been engineered to fluoresce upon chondrocyte differentiation were treated with combinations of factors necessary for chondrogenesis, and chondrocyte differentiation was detected as fluorescence. We screened for the combination that could induce fluorescence within 3 days. Then, primary mesenchymal stem cells, nonchondrogenic immortalized cell lines, and primary dermal fibroblasts were treated with the combination, and the induction of chondrocyte differentiation was assessed by detecting the expression of the cartilage marker genes and the accumulation of proteoglycan-rich matrix. The effects of monolayer, spheroid, and 3-dimensional culture systems on induction by combinations of transcription factors were compared. The effects of the combination on hypertrophic and osteoblastic differentiation were evaluated by detecting the expression of the characteristic marker genes.**

Results. **No single factor induced fluorescence. Among various combinations examined, only the SOX5, SOX6, and SOX9 combination (the SOX trio) induced fluorescence within 3 days. The SOX trio successfully induced chondrocyte differentiation in all cell types tested, including nonchondrogenic types, and the induction occurred regardless of the culture system used. Contrary to the conventional chondrogenic techniques, the SOX trio suppressed hypertrophic and osteogenic differentiation at the same time.**

Conclusion. **These data strongly suggest that the SOX trio provides signals sufficient for the induction of permanent cartilage.**

Utilizing the differentiation and proliferation capabilities of stem cells, regenerative medicine attempts to treat irreversible organ failures that cannot be dealt with by conventional medical treatment. In the skeletal area, cartilage has a relatively poor regenerative capacity and, thus, may benefit most from regenerative medicine. Conditions such as osteoarthritis and congenital skeletal defects are apparent targets that have great medical and socioeconomic impact. To make cartilage regenerative medicine a reality, it is essential to know the conditions that are both necessary and sufficient for chondrogenesis.

A number of factors have been shown to be vital for chondrogenesis. These factors include the sex-determining region Y–type high mobility group box (SOX) family of transcription factors (1), insulin-like growth factor 1 (IGF-1) (2), fibroblast growth factor 2 (FGF-2) (3), Indian hedgehog (IHH) (4), bone morpho-

Dr. Ikegawa's work was supported by a grant from the Japanese Millennium Project and a Grant-in-Aid for Scientific Research from the Japanese Ministry of Education, Culture, Sports, Science, and Technology (14207055). Dr. Chung's work was supported by a Grant-in-Aid for Scientific Research from the Japanese Ministry of Education, Culture, Sports, Science, and Technology (15390452) and by a generous endowment from Takeda Chemical Industries, Osaka, Japan.

[1]Toshiyuki Ikeda, MD, Akihiko Mabuchi, MD, Ikuyo Kou, MEng, Shoji Seki, MD, Shiro Ikegawa, MD, PhD: SNP Research Center, RIKEN (The Institute of Physical and Chemical Research), Tokyo, Japan; [2]Satoru Kamekura, MD, Kozo Nakamura, MD, PhD, Hiroshi Kawaguchi, MD, PhD: University of Tokyo Graduate School of Medicine, Tokyo, Japan; [3]Tsuyoshi Takato, MD, PhD, Ung-il Chung, MD, PhD: University of Tokyo Hospital, Tokyo, Japan.

Address correspondence and reprint requests to Shiro Ikegawa, MD, PhD: Laboratory for Bone and Joint Diseases, SNP Research Center, RIKEN, c/o Institute of Medical Science, University of Tokyo, 4-6-1 Shirokanedai, Minato-ku, Tokyo 108-8639, Japan. E-mail: sikegawa@ims.u-tokyo.ac.jp.

Submitted for publication February 25, 2004; accepted in revised form August 2, 2004.

genetic protein 2 (BMP-2) (5), transforming growth factor β (TGFβ) (6), and Wnt proteins (4).

Many lines of evidence, both in vitro and in vivo, have shown that SOX proteins are necessary for chondrogenesis. SOX9 is expressed in all chondroprogenitors and chondrocytes except hypertrophic chondrocytes (7,8). Heterozygous mutations of *SOX9* cause a severe chondrodysplasia, known as campomelic dysplasia, in humans (9,10). Analysis of chimeric mice containing wild-type and *Sox9*-deficient cells showed that the mutant cells were excluded from chondrogenic mesenchymal condensation and failed to express chondrocyte-specific marker genes (11). SOX9 was shown to bind to and activate chondrocyte-specific enhancer elements in *Col2a1*, *Col9a1*, *Col11a2*, and *Aggrecan* in vitro (12–18). Conditional ablation of the *Sox9* gene in limb buds before mesenchymal condensation resulted in a complete absence of chondrocytes, whereas conditional ablation of *Sox9* after mesenchymal condensation resulted in a severe generalized chondrodysplasia (19). Two other members of the Sox family, Sox5 and Sox6, are also required for chondrogenesis. $Sox5^{-/-}$ and $Sox6^{-/-}$ mice show chondrodysplastic phenotypes and die at birth. $Sox5^{-/-}$ and $Sox6^{-/-}$ mice develop a severe, generalized chondrodysplasia characterized by a virtual absence of cartilage (20). In vitro studies have shown that Sox5 and Sox6 cooperate with Sox9 to activate the *Col2a1* enhancer in chondrogenic cells (21).

Although these lines of evidence demonstrate that these factors are necessary for chondrogenesis, no single factor has proved sufficient for the process. That is, we do not yet know what constitutes a sufficient signal for chondrogenesis. In the current study, we sought to determine the sufficient signal by screening various combinations of known factors that are necessary for chondrogenesis.

MATERIALS AND METHODS

Construction of plasmid vectors and adenoviruses. Combinations of known factors important for chondrogenesis were screened. These factors included SOX5, SOX6, SOX9, IGF-1, FGF-2, IHH, BMP-2, TGFβ, and Wnt proteins. For each signaling pathway, we constructed an adenovirus vector that stimulates the pathway (overexpression of the wild-type form or expression of the constitutively active form) as well as one that inhibits the pathway (expression of the dominant-negative form or RNA interference [RNAi] form).

We then stimulated the signaling and inhibition of each factor. SOX signaling was stimulated as described below. To stimulate SOX inhibition, we constructed adenoviruses expressing RNAi for SOX5, SOX6, and SOX9 (22). To stimulate IGF-1 signaling, we used an adenovirus expressing insulin receptor substrate 1 (IRS-1); to inhibit, we used one expressing a dominant-negative form of IRS-1 (23). To stimulate FGF signaling, we constructed an adenovirus expressing a constitutively active form of FGF receptor 3 (FGFR-3); to inhibit, we used one expressing RNAi for FGFR-3 (24). To stimulate IHH signaling, we constructed an adenovirus expressing constitutively active Smoothened (25); to inhibit, we used one expressing a repressor form of Gli-3 (26). To stimulate BMP signaling, we used an adenovirus expressing a constitutively active form of activin receptor–like kinase 6 (ALK-6); to inhibit, we used one expressing Smad6 (27). To stimulate TGFβ signaling, we used an adenovirus expressing a constitutively active form of ALK-5; to inhibit, we used one expressing Smad7 (27). To stimulate Wnt signaling, we constructed an adenovirus expressing a constitutively active form of T cell factor (TCF); to inhibit, we used one expressing a dominant-negative form of TCF (28).

As a control vector, we used the adenovirus expressing the β-galactosidase gene *lacZ*. Thus, for each signaling pathway, there were 3 adenoviruses (positive, negative, and neutral). To create combinations, one adenovirus from each signaling pathway was selected and mixed with another.

To create adenoviruses expressing SOX5, SOX6, and SOX9, full-length human *SOX5*, *SOX6*, and *SOX9* complementary DNA (cDNA) was amplified by polymerase chain reaction (PCR) and cloned into pEGFPC1 and pShuttle mammalian expression vectors (Clontech, Palo Alto, CA). We confirmed that the introduced green fluorescence protein (GFP) tags did not interfere with the activities of any SOX. PCR products were verified by DNA sequencing. Adenovirus vectors expressing SOX5, SOX6, and SOX9 were constructed with the AdenoX Expression system (Clontech), according to the manufacturer's instructions. Adenovirus vector expressing LacZ was provided by the manufacturer. Adenoviruses were packaged and amplified in HEK 293 cells and purified with an AdenoX virus purification kit (Clontech). The viral titers were estimated with an AdenoX rapid titer assay kit (Clontech).

Isolation and culture of cells. Mouse embryonic stem (ES) cells were isolated from blastocysts obtained from C57BL/6 mice expressing a GFP transgene engineered to be expressed specifically in chondrocytes (*Col2-GFP*), as previously described (29). *Col2-GFP* ES cells were cultured in high-glucose Dulbecco's modified Eagle's medium (DMEM; Sigma, St. Louis, MO) supplemented with β-mercaptoethanol (100 μM), leukemia inhibitory factor (1,000 units/ml), nonessential amino acids (1%), penicillin (50 units/ml), streptomycin (50 μg/ml), and fetal bovine serum (FBS; 15%) (JRH Biosciences, Lenexa, KS), as previously described (30). To generate *Col2-GFP* mice, the 6.3-kb *Col2a1* promoter region directing chondrocyte-specific expression was released from the plasmid p3000i3020Col2a1 (a generous gift from Dr. Benoit de Crombrugghe, M. D. Anderson Cancer Center, Houston, TX) and subcloned into the pEGFP-1 vector (Clontech). The *Col2-GFP* transgene was then excised and purified for microinjection. Pronuclear injection and subsequent selection of founders were performed as previously described (31).

Human mesenchymal stem cells (MSCs) and adult human dermal fibroblasts (DFs) were purchased from Cambrex (East Rutherford, NJ). Human MSCs were cultured in MSC growth medium at 37°C under 5% CO_2. Adult human DFs were cultured in high-glucose DMEM supplemented with